THE ROYAL SOCIETY

# Design of novel magnets using Prussian blue analogues

By Kazuhito Hashimoto and Shin-ichi Ohkoshi

*Research Center for Advanced Science and Technology, The University of Tokyo, 4-6-1 Komaba, Meguro-ku, Tokyo 153-8904, Japan*

The main aim of this paper is to show how well we can design novel molecule-based magnets using Prussian blue analogues based on theory. We obtained various novel magnets, i.e. magnets containing both ferro- and antiferromagnetic interactions without spin frustration, a magnet having two compensation temperatures, coloured transparent magnets, a photomagnet and a photoinduced pole inversion magnet. These magnets were designed using simple theories, including molecular field theory.

**Keywords: molecule-based magnet; Prussian blue; photomagnet; pole inversion; molecular field theory; supercharge interaction**

## 1. Introduction

Control of magnetic properties is an attractive but very difficult problem in the field of magnetic materials. Although the theoretical analyses of various magnetic properties of materials are often successful in great detail, theoretical prediction for the production of novel magnets is difficult in general and especially for classical metal or metal oxide magnets. One of the main reasons is that various types of exchange and/or superexchange interactions exist among many spin sources. Moreover, metal or metal ion substitution often causes structural distortions. For molecule-based magnets, however, theoretical design could become more useful than for the classical magnets, because the molecular magnets can be obtained through a selection of appropriate spin sources (see Gatteschi *et al*. 1991; Kahn 1993; Miller & Epstein 1994). This is especially appropriate for Prussian blue analogues, some of which become ferromagnets, e.g. $CsNi[Cr(CN)_6]$, $T_c = 90$ K (Entley & Girolami 1994), while others are ferrimagnets, e.g. $V_{1.16}[Cr(CN)_6]$, $T_c = 315$ K (Ferlay *et al*. 1995), where the theoretical prediction of magnetic properties is very useful, as shown later. Let us consider the magnetic coupling of the metal centres in Prussian blue analogues. The coupling cannot be explained either by weak dipole–dipole interactions or by direct exchange interactions via overlapping metal orbitals. The coupling is described in terms of a superexchange mechanism through the cyanide ligands. The superexchange mechanism is summarized on the basis of the Goodenough–Kanamori rule that includes consideration of the bond angle and the symmetry of the metal and ligand orbitals concerned (see Goodenough 1958, 1959; Kanamori 1959). There are two mechanisms for superexchange interactions: the kinetic exchange mechanism ($J_{KE}$) and the potential exchange mechanism ($J_{PE}$) (figure 1*a*) (see Ginsberg 1971). On the one hand, kinetic exchange is mediated by a direct pathway of the overlapping orbitals, which connects the two interacting magnetic orbitals. It is antiferromagnetic in nature as

a consequence of the Pauli principle, leading to an antiparallel spin ordering via a common covalent bond. On the other hand, potential exchange is effective between orthogonal magnetic orbitals with comparable orbital energy. In this case Hund's rule leads to a parallel spin alignment, i.e. a ferromagnetic interaction. In the case of Prussian blue analogues, the metal d-orbitals are split into $t_{2g}$ and $e_g$ sets by the CN ligands (figure 1*b*). Moreover, in most cases, they maintain their face-centred cubic (FCC) structure even after substituting the metal ions. Therefore, based on magnetic orbital symmetry, we can understand whether the orbital superexchange among each orbital on the metal ions is $J_{KE}$ or $J_{PE}$. When the magnetic orbital symmetries of the metals are the same, the superexchange interaction might be $J_{KE}$. Conversely, when the magnetic orbital symmetries of the metals are different, the superexchange interaction might be $J_{PE}$. The total superexchange interaction is given by the sum of all the orbital exchange contributions between transition metal ions (see Ginsberg 1971; Nishino *et al*. 1997).

For example, consider the case of the hexacyanochromate cyanide $A^{II}_y[Cr^{III}(CN)_6]$, with $Cr^{III}$ being $(t_{2g})^3$ and $S_{Cr} = 3/2$. If each magnetic orbital of $A^{II}$ has $e_g$ symmetry, there is no overlap between the $Cr^{III}$ and $A^{II}$ magnetic orbitals. In this situation, the potential exchange mechanism becomes dominant, leading to a ferromagnetic interaction between $Cr^{III}$ and $A^{II}$. In fact, in $CsNi^{II}[Cr^{III}(CN)_6]$, with a high-spin state for $Ni^{II}$ ($(t_{2g})^6(e_g)^2$, $S_{Ni} = 1$), a ferromagnetic interaction operates between $Cr^{III}$ and $Ni^{II}$, as reported by Entley & Girolami (1994). However, when each $A^{II}$ magnetic orbital has $t_{2g}$ symmetry, the overlap between the $t_{2g}$(A) and $t_{2g}$(Cr) orbitals gives rise to kinetic exchange, leading to an antiferromagnetic interaction. If both $t_{2g}$ and $e_g$ electrons are present on $A^{II}$, the superexchange coupling constant ($J_{AB}$) is described as the sum of the ferromagnetic ($J_{PE} > 0$) and antiferromagnetic ($J_{KE} < 0$) orbital contributions. Kinetic exchange usually operates in preference to potential exchange, i.e. $|J_{KE}| > |J_{PE}|$ (see Anderson 1959). For example, Griebler & Babel (1982) showed that the interaction between $Cr^{III}$ and $Mn^{II}$ with a high-spin state for $Mn^{II}$ ($(t_{2g})^3(e_g)^2$, $S_{Mn} = 5/2$) in $CsMn^{II}[Cr^{III}(CN)_6]$ is antiferromagnetic, and the compound is a ferrimagnet. In most Prussian blue analogues, therefore, we can readily understand the superexchange interactions.

## 2. Design of the superexchange interactions

Here, we will discuss the magnetic properties of Prussian blue analogues containing both ferromagnetic and antiferromagnetic interactions (see Ohkoshi *et al*. 1997*a*, *b*). The magnets have both ferromagnetic and ferrimagnetic characteristics simultaneously, and therefore could be called mixed ferro-ferrimagnets. It may be difficult to achieve such properties in classical metal oxide magnets, because various types of magnetic interactions involving the metal ions can operate in these systems, including superexchange interactions, direct exchange interactions, and dipole–dipole interactions. In Prussian blue analogues, however, their FCC structure and the relatively long distance between magnetic ions make it possible for ferromagnetic and antiferromagnetic interactions to exist independently. As prototypes exemplifying the mixed ferro-ferrimagnetism, we will discuss a series of $(Ni^{II}_xMn^{II}_{1-x})_{1.5}[Cr^{III}(CN)_6]$ compounds, which can accommodate both ferromagnetic ($J_{NiCr} > 0$) and antiferromagnetic ($J_{MnCr} < 0$) exchange interactions (figure 2).

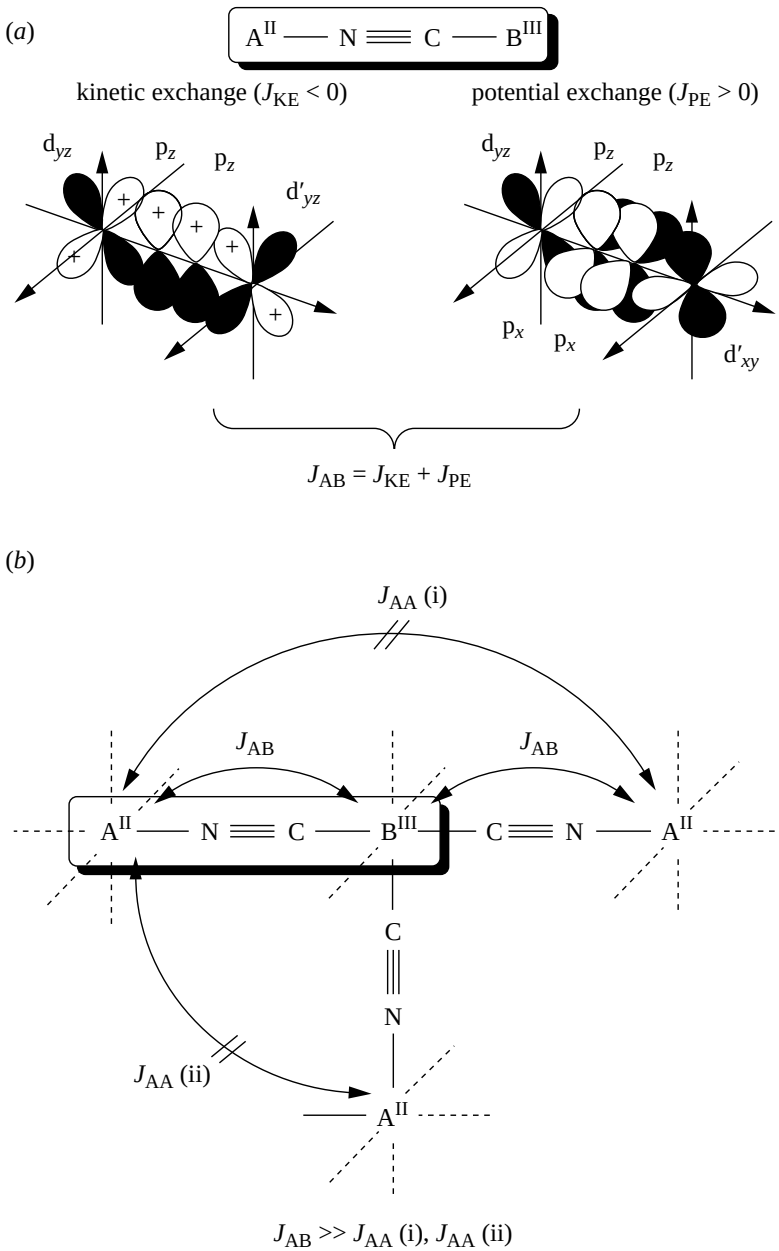


Figure 1. (*a*) The two basic mechanisms for the isotropic exchange in the magnetic coupling between the $A^{II}$ and $B^{III}$ ions in the CN-bridged complex. On the left is one of the significant kinetic exchange ($J_{KE}$) pathways ($d_{yz}\|\pi_z\|d_{yz'}$), and on the right is one of significant potential exchange ($J_{PE}$) pathways ($d_{yz}\|\pi_z \perp \pi_x\|d_{xy'}$). The superexchange coupling between $A^{II}$ and $B^{III}$ ($J_{AB}$) involves a superposition of $J_{PE}$ and $J_{KE}$. (*b*) In the Prussian blue structure, superexchange interactions at a 180° angle between $A^{II}$ and $B^{III}$ are dominant over superexchange interactions of the second nearest-neighbour metals ($J_{AA(i)}$) and direct exchange interactions ($J_{AA(ii)}$).

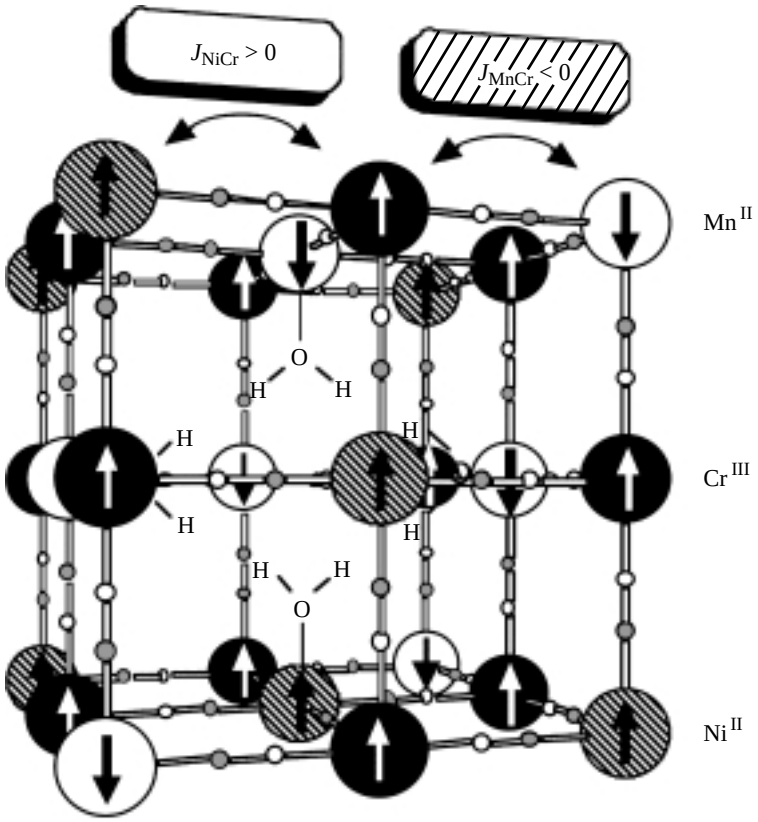


Figure 2. Schematic illustration of a ternary metal Prussian blue analogue containing both ferromagnetic and antiferromagnetic interactions. $Cr^{III}$ and either $Ni^{II}$ or $Mn^{II}$, which are randomly incorporated in the lattice, are linked in an alternating fashion.

Let us evaluate the theoretical saturation magnetization ($I_s$) values for materials. We first consider the model compounds, $Ni^{II}_{1.5}[Cr^{III}(CN)_6]$ ferromagnet and $Mn^{II}_{1.5}[Cr^{III}(CN)_6]$ ferrimagnet. The $I_s$ values of these two compounds are expected to be $6\mu_B$ (due to parallel alignment of the spins, $S_{Ni} = 1$ and $S_{Cr} = 3/2$) and $4.5\mu_B$ (due to antiparallel alignment of the spins, $S_{Mn} = 5/2$ and $S_{Cr} = 3/2$), respectively. When powders of the two compounds are physically mixed, the total $I_s$ will vary between 4.5 and $6\mu_B$, depending on the mixing ratio, as shown in figure 3 (dashed line). However, when the two compounds are mixed at an atomic level, parallel spins ($Ni^{II}$ and $Cr^{III}$) and antiparallel spins ($Mn^{II}$ and $Cr^{III}$) can partly or even completely cancel, depending on the mixing ratio, because $Cr^{III}$ and either $Ni^{II}$ or $Mn^{II}$ are linked in an alternating fashion. In this manner, materials with $I_s$ values anywhere in the range 0–$6\mu_B$ may be prepared. For the members of the series $(Ni^{II}_x Mn^{II}_{1-x})_{1.5}[Cr^{III}(CN)_6]$, $I_s$ is given by

$$I_s = g\mu_B|S_{Cr} + 1.5[S_{Ni}x - S_{Mn}(1-x)]|. \tag{2.1}$$

The calculated dependence of $I_s$ on $x$ is shown in figure 3 (solid line). The $I_s$ is predicted to vanish for $x = 3/7$ (0.428), and such a material should exhibit antiferromagnetic properties. Moreover, spin glass behaviour does not occur in this series

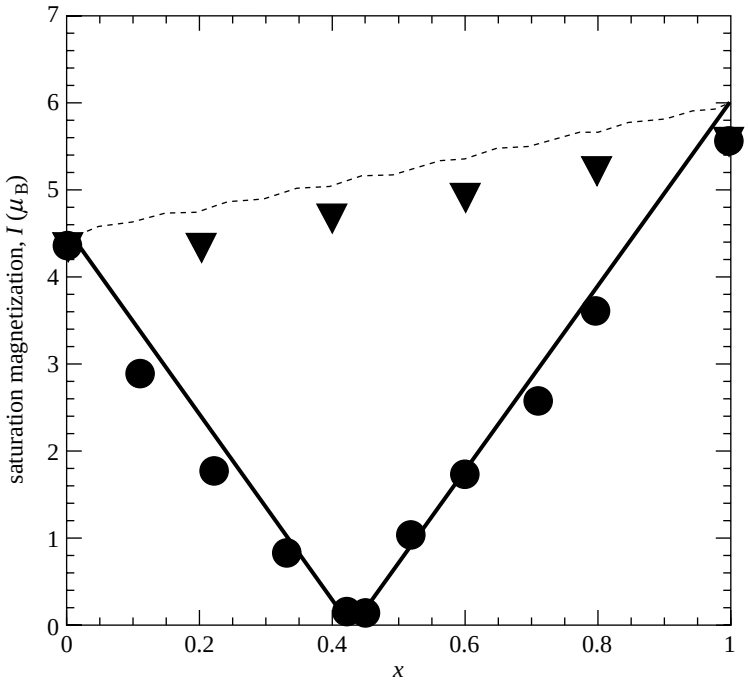


Figure 3. Calculated and experimentally observed saturation magnetizations as a function of $x$. Atomic-level mixture $(Ni^{II}_x Mn^{II}_{1-x})_{1.5}[Cr^{III}(CN)_6] \cdot zH_2O$: theory (——), observed (•). Macroscopic physical mixture $x \cdot Ni^{II}_{1.5}[Cr^{III}(CN)_6] + (1-x) \cdot Mn^{II}_{1.5}[Cr^{III}(CN)_6]$: calculated (– – – –); observed (▼).

because the direction of each spin is consistent with the sign of $J$ of the nearest-neighbour spin site.

These compounds can be prepared by reacting mixtures of $NiCl_2$ and $MnCl_2$ aqueous solutions (with a given molar ratio $x_{mix}$, ranging from zero to unity, of $Ni^{2+}$ versus the total of $Ni^{2+}$ and $Mn^{2+}$) with $K_3Cr(CN)_6$ aqueous solution to yield green precipitates. The $x$ values in the resulting precipitates are in general in good agreement with the $x_{mix}$ values used in the syntheses. The results for the X-ray powder diffraction measurements show that patterns for each member of the series are consistent with FCC structure, with the lattice constant decreasing from 10.787 to 10.467 Å with increasing $x$, and that the materials are not macroscopic mixtures of $Ni^{II}_{1.5}[Cr^{III}(CN)_6]$ and $Mn^{II}_{1.5}[Cr^{III}(CN)_6]$, but are ternary metal complexes in which $Mn^{II}$ and $Ni^{II}$ are randomly incorporated in the lattice, corresponding to the mixing ratio of $NiCl_2$ and $MnCl_2$. It is important to note that the carbon atoms of the cyano groups are always bonded to $Cr^{III}$, and the nitrogen atoms are always bonded to either $Ni^{II}$ or $Mn^{II}$.

The observed $I_s$ values of $Ni^{II}_{1.5}[Cr^{III}(CN)_6]$ and $Mn^{II}_{1.5}[Cr^{III}(CN)_6]$ are 5.57 and $4.38\mu_B$ for a given formula, respectively. When powders of the two compounds are physically mixed, the total $I_s$ varied between 4.38 and $5.57\mu_B$, depending on the mixing ratio, as shown in figure 3 (triangles). Conversely, when the two compounds are mixed at an atomic level, those for the intermediate compositions varied in a systematic fashion as a function of $x$ (figure 3, filled circles). Minimum values are

obtained for $x$ values close to 3/7 (0.42 and 0.45); the molar $I_s$ values are very close to zero, just at the point where parallel spins ($Cr^{III}$ and $Ni^{II}$) and antiparallel spins ($Mn^{II}$) should completely cancel out. Thus it can be noticed that the molar $I_s$ dependence on $x$ follows equation (2.1) quite well. The Weiss temperature ($\theta_C$) values increase monotonically from negative to positive values with increasing $x$, and this behaviour can be explained by considering that the weighted average of $J_{NiCr}$ and $J_{MnCr}$ changes as a function of $x$.

The other magnetic properties are also changed depending on $x$, but one of the most interesting aspects of the magnetic behaviour of this series is the thermodynamics of the magnetization. In general, ferromagnets exhibit monotonically increasing magnetization curves with decreasing temperature below $T_C$. However, in the case of ferrimagnets, Néel (1948) envisaged the possibility that saturation magnetization versus temperature curves could be classified into four types according to the shape, i.e. Q-, R-, P- and N-types. The Q- and R-type curves exhibit monotonic increases with decreasing temperature, while the P-type exhibits a single maximum and the N-type exhibits two maxima. For the present mixed ferro-ferrimagnets, all these four types of temperature dependence are observed with one series of compounds. In figure 4*a* are shown the magnetization versus temperature curves at 1000 G with various $x$ values. These types of curves are consistent with the Néel classification, Type R ($x = 0$), Type N ($x = 0.38$), Type P ($x = 0.45$), and Type Q ($x = 1$). In addition, the magnetization of the compound for $0.33 < x < 0.43$ shows a negative value when the external magnetic field is lower than its coercive field (figure 5*a*). The temperature at which the magnetization becomes zero is called a compensation temperature ($T_{comp}$) (see Gorter 1954; Mathonière *et al.* 1994).

These temperature dependencies can be analysed using a molecular field (MF) theory (see Anderson 1964), considering only two types of superexchange couplings between the nearest-neighbour sites, one for Ni–Cr and the other for Mn–Cr, according to the model shown in figure 2. Those between the second nearest-neighbour sites (Mn–Ni and Cr–Cr) are neglected. The molecular fields $H_{Ni}$, $H_{Mn}$ and $H_{Cr}$ acting on the three sublattice sites in $(Ni^{II}_x Mn^{II}_{1-x})_{1.5}[Cr^{III}(CN)_6]$ can be expressed as follows:

$$H_{Mn} = H_0 + n_{MnCr} M_{Cr}, \tag{2.2}$$

$$H_{Ni} = H_0 + n_{NiCr} M_{Cr}, \tag{2.3}$$

$$H_{Cr} = H_0 + n_{CrMn} M_{Mn} + n_{CrNi} M_{Ni}, \tag{2.4}$$

where $H_0$ is the external magnetic field, $n_{ij}$ are the MF coefficients, and $M_{Ni}$, $M_{Mn}$ and $M_{Cr}$ are the sublattice magnetizations per unit volume for the Ni, Mn and Cr sites, respectively. The MF coefficients $n_{ij}$ are related to the exchange coefficients ($J_{ij}$) by

$$n_{MnCr} = 2Z_{MnCr} J_{MnCr}/(\mu N (g\mu_B)^2), \tag{2.5}$$

$$n_{NiCr} = 2Z_{NiCr} J_{NiCr}/(\mu N (g\mu_B)^2), \tag{2.6}$$

$$n_{CrMn} = 2Z_{CrMn} J_{MnCr}/(\lambda(1-x) N (g\mu_B)^2), \tag{2.7}$$

$$n_{CrNi} = 2Z_{CrNi} J_{NiCr}/(\lambda x N (g\mu_B)^2), \tag{2.8}$$

where $\mu_B$ is the Bohr magneton, $Z_{ij}$ are the numbers of the nearest-neighbour $j$-site ions surrounding an $i$-site ion, $N$ is the total number of all types of metal ions per unit volume, and $\lambda$ and $\mu$ represent the molar fractions for the $A^{II}$ cations (total of

the molar fractions for $Mn^{II}$ and $Ni^{II}$) ions and for the $Cr^{III}$ ions, respectively. When we designate the thermally averaged values of the spins of the Mn, Ni and Cr ions in their respective sites in the direction of each sublattice magnetization as $\langle S_{\mathrm{Mn}}\rangle$, $\langle S_{\mathrm{Ni}}\rangle$ and $\langle S_{\mathrm{Cr}}\rangle$, the sublattice magnetization can be expressed as follows:

$$M_{\mathrm{Mn}} = \lambda(1-x)Ng\mu_{\mathrm{B}}\langle S_{\mathrm{Mn}}\rangle, \tag{2.9}$$

$$M_{\mathrm{Ni}} = \lambda x Ng\mu_{\mathrm{B}}\langle S_{\mathrm{Ni}}\rangle, \tag{2.10}$$

$$M_{\mathrm{Cr}} = \mu Ng\mu_{\mathrm{B}}\langle S_{\mathrm{Cr}}\rangle. \tag{2.11}$$

Substituting (2.5)–(2.8) and (2.9)–(2.11) into (2.2)–(2.4), we have

$$H_{\mathrm{Mn}} = H_0 + 2Z_{\mathrm{MnCr}}J_{\mathrm{MnCr}}\langle S_{\mathrm{Cr}}\rangle/g\mu_{\mathrm{B}}, \tag{2.12}$$

$$H_{\mathrm{Ni}} = H_0 + 2Z_{\mathrm{NiCr}}J_{\mathrm{NiCr}}\langle S_{\mathrm{Cr}}\rangle/g\mu_{\mathrm{B}}, \tag{2.13}$$

$$H_{\mathrm{Cr}} = H_0 + 2Z_{\mathrm{CrMn}}(1-x)J_{\mathrm{MnCr}}\langle S_{\mathrm{Mn}}\rangle/g\mu_{\mathrm{B}} + 2Z_{\mathrm{CrNi}}xJ_{\mathrm{NiCr}}\langle S_{\mathrm{Ni}}\rangle/g\mu_{\mathrm{B}}. \tag{2.14}$$

The magnitudes of $\langle S_{\mathrm{Mn}}\rangle$, $\langle S_{\mathrm{Ni}}\rangle$ and $\langle S_{\mathrm{Cr}}\rangle$, setting $H_0 = 0$, are given by

$$\langle S_{\mathrm{Mn}}\rangle = S_{\mathrm{Mn0}}B_{\mathrm{SMn0}}(2Z_{\mathrm{MnCr}}J_{\mathrm{MnCr}}S_{\mathrm{Mn0}}\langle S_{\mathrm{Cr}}\rangle/k_{\mathrm{B}}T), \tag{2.15}$$

$$\langle S_{\mathrm{Ni}}\rangle = S_{\mathrm{Ni0}}B_{\mathrm{SNi0}}(2Z_{\mathrm{NiCr}}J_{\mathrm{NiCr}}S_{\mathrm{Ni0}}\langle S_{\mathrm{Cr}}\rangle/k_{\mathrm{B}}T), \tag{2.16}$$

$$\langle S_{\mathrm{Cr}}\rangle = S_{\mathrm{Cr0}}B_{\mathrm{SCr0}}(2Z_{\mathrm{CrMn}}(1-x)J_{\mathrm{MnCr}}S_{\mathrm{Cr0}}\langle S_{\mathrm{Mn}}\rangle/k_{\mathrm{B}}T + 2Z_{\mathrm{CrNi}}xJ_{\mathrm{MnCr}}S_{\mathrm{Cr0}}\langle S_{\mathrm{Ni}}\rangle/k_{\mathrm{B}}T), \tag{2.17}$$

where $B_{\mathrm{S}}$ is the Brillouin function, $S_{\mathrm{Mn0}}$, $S_{\mathrm{Ni0}}$ and $S_{\mathrm{Cr0}}$ are the values of $\langle S_{\mathrm{Mn}}\rangle$, $\langle S_{\mathrm{Ni}}\rangle$ and $\langle S_{\mathrm{Cr}}\rangle$ at $T = 0\,\mathrm{K}$ and $k_{\mathrm{B}}$ is the Boltzmann constant. The $\langle S_{\mathrm{Mn}}\rangle$, $\langle S_{\mathrm{Ni}}\rangle$ and $\langle S_{\mathrm{Cr}}\rangle$ can be calculated numerically. The total magnetization ($M_{\mathrm{total}}$) is

$$\begin{aligned} M_{\mathrm{total}} &= -M_{\mathrm{Mn}} + M_{\mathrm{Ni}} + M_{\mathrm{Cr}} \\ &= Ng\mu_{\mathrm{B}}[-\lambda(1-x)\langle S_{\mathrm{Mn}}\rangle + \lambda x\langle S_{\mathrm{Ni}}\rangle + \mu\langle S_{\mathrm{Cr}}\rangle]. \end{aligned} \tag{2.18}$$

The negative and positive signs are for antiparallel and parallel interactions, respectively. For $(Ni^{II}_{x}Mn^{II}_{1-x})_{1.5}[Cr^{III}(CN)_6]\cdot 7.5H_2O$, the numbers of the nearest neighbours $Z_{ij}$ are $Z_{\mathrm{MnCr}} = Z_{\mathrm{NiCr}} = 4$; $Z_{\mathrm{CrMn}} = 6(1-x)$, $Z_{\mathrm{CrNi}} = 6x$; and other quantities are as follows: $\lambda = 1.5$; $\mu = 1$; $S_{\mathrm{Mn0}} = 5/2$; $S_{\mathrm{Ni0}} = 1$; $S_{\mathrm{Cr0}} = 3/2$; and $g = 2$.

In order to calculate the temperature dependence, the $J$ values of $Mn^{II}$–$Cr^{III}$ and $Ni^{II}$–$Cr^{III}$ must be estimated. These values can be obtained approximately from the observed $T_{\mathrm{c}}$ values for $Mn^{II}_{1.5}[Cr^{III}(CN)_6]$ and $Ni^{II}_{1.5}[Cr^{III}(CN)_6]$. The relationship between the $T_{\mathrm{c}}$ values for the Prussian blue analogues and the $J$ values is expressed as follows:

$$T_{\mathrm{c}} = 2(Z_{ij}Z_{ji})^{1/2}|J_{ij}|(S_i(S_i+1)S_j(S_j+1))^{1/2}/3k_{\mathrm{B}}, \tag{2.19}$$

where $i$ = Ni or Mn and $j$ = Cr. Based on this equation, $J_{\mathrm{NiCr}} = 5.6\,\mathrm{cm}^{-1}$ and $J_{\mathrm{MnCr}} = -2.5\,\mathrm{cm}^{-1}$ are obtained, using $T_{\mathrm{c}}$ values of a 72 K for $Ni^{II}_{1.5}[Cr^{III}(CN)_6]\cdot 8H_2O$ and a 67 K for $Mn^{II}_{1.5}[Cr^{III}(CN)_6]\cdot 7.5H_2O$.

For the calculation of magnetization dependencies in the

$$(Ni^{II}_{x}Mn^{II}_{1-x})_{1.5}[Cr^{III}(CN)_6]\cdot zH_2O$$

series, the magnetizations of Ni and Cr are expected to be along the direction of the external magnetic field, because experimental curves shown here are obtained

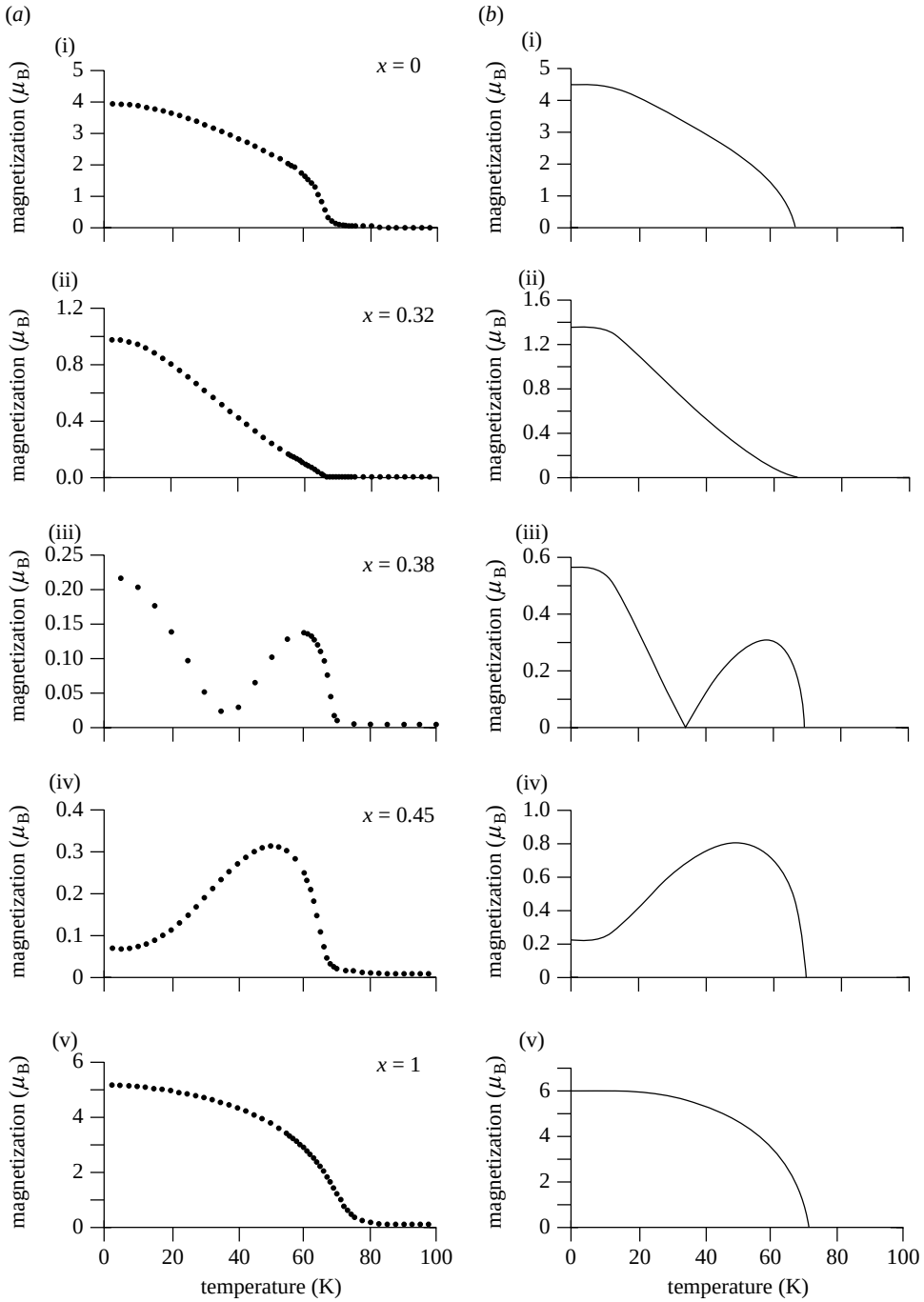


Figure 4. Magnetization versus temperature curves for $(Ni_x^{II}Mn_{1-x}^{II})_{1.5}[Cr^{III}(CN)_6] \cdot zH_2O$: (*a*) experimental points obtained at 1000 G and (*b*) calculated dependence of $|M_{total}|$ based on molecular field theory, assuming three sublattices, the two $J$ coefficients ($J_{NiCr} = 5.6\ cm^{-1}$ and $J_{MnCr} = -2.5\ cm^{-1}$), and the compositional parameter $x$.

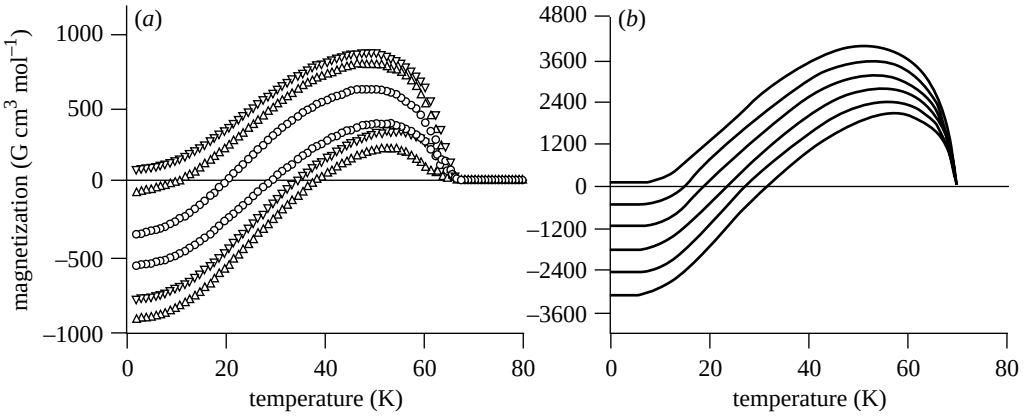


Figure 5. Magnetization versus temperature curves for $(Ni^{II}_{x}Mn^{II}_{1-x})_{1.5}[Cr^{III}(CN)_6] \cdot zH_2O$ ($x = 0.38$, 0.39, 0.40, 0.41, 0.42, 0.43, going from the lowest curve to the highest curve). (*a*) Experimental data obtained at 10 G and (*b*) calculated temperature dependences of magnetization $M_{\mathrm{total}}$ based on molecular field theory, with three sublattice sites (Ni, Mn, Cr), with $J$ coefficients $J_{\mathrm{NiCr}} = 5.6\ \mathrm{cm}^{-1}$ and $J_{\mathrm{MnCr}} = -2.5\ \mathrm{cm}^{-1}$.

by a field cooling (10 G or 1000 G) method and the $T_{\mathrm{c}}$ value for $Ni^{II}_{1.5}[Cr^{III}(CN)_6]$ is higher than that for $Mn^{II}_{1.5}[Cr^{III}(CN)_6]$. Therefore, in this system, the signs of the magnetization of ferromagnetic sites (Ni and Cr) can be assumed to be positive. Note that the calculated spontaneous magnetizations are essentially the saturated values, because the MF theory does not consider the magnetization process. The negative magnetization below $T_{\mathrm{comp}}$ is compelled to invert along the external magnetic field direction when the external magnetic field is larger. Therefore, for simulations of observed temperature dependence curves at 10 G and 1000 G, the $M_{\mathrm{total}}$ and the $|M_{\mathrm{total}}|$ curves are adopted, respectively.

Under these conditions, the temperature dependencies of the spontaneous magnetization are calculated for several different compositions. For $x = 0$, only $J_{\mathrm{MnCr}}$ appears in the equation, and hence the curve exhibits a monotonically increasing magnetization with decreasing temperature. For $0.33 < x < 3/7$ (0.429), the $|M_{\mathrm{total}}|$ curves exhibit two maxima, with a minimum at $T_{\mathrm{comp}}$ (see curve for $x = 0.38$ in figure 4*b*). This $T_{\mathrm{comp}}$ shifts from $T_{\mathrm{c}}$ to 0 K with increasing $x$. On the other hand, $M_{\mathrm{total}}$ for $0.33 < x < 3/7$ exhibits negative magnetization with $T_{\mathrm{comp}}$ (figure 5*b*). For $x = 3/7$, $T_{\mathrm{comp}}$ was 0 K, and this value corresponds to that predicted by equation (2.1), in which the saturation magnetization disappears. For $x > 0.45$, the curve exhibits a single maximum. For $x = 1$, the curve exhibits a monotonic increase due to the fact that only $J_{\mathrm{NiCr}}$ appears. The calculated curves for $|M_{\mathrm{total}}|$ and $M_{\mathrm{total}}$ qualitatively reproduce the experimental ones at 1000 G and 10 G, as shown in figures 4 and 5, respectively.

These various types of temperature dependence of the magnetization arise because the negative magnetization due to the $Mn^{II}$ sublattice and the positive magnetizations due to the $Ni^{II}$ and $Cr^{III}$ sublattices have different temperature dependencies (figure 6*a*). For example, for $x = 0.38$, the relations of the magnitude among each sublattice magnetizations are as follows: $|M_{\mathrm{Ni}}| + |M_{\mathrm{Cr}}| > |M_{\mathrm{Mn}}|$ at $T > T_{\mathrm{comp}}$ and $|M_{\mathrm{Ni}}| + |M_{\mathrm{Cr}}| < |M_{\mathrm{Mn}}|$ at $T < T_{\mathrm{comp}}$, respectively (figure 6*b*). The close correspondence between the calculated and observed curves shows that the magnetic properties

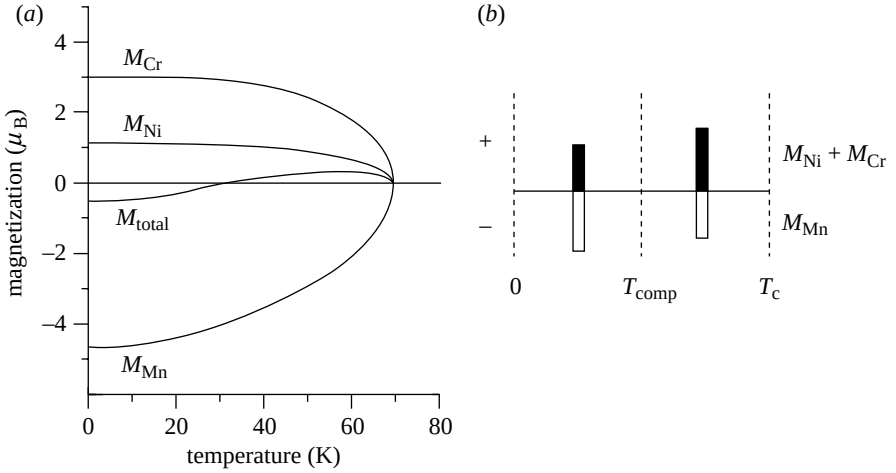


Figure 6. (*a*) Calculated temperature-dependence curves for each sublattice ($M_{Mn}$, $M_{Ni}$, $M_{Cr}$) and total magnetization ($M_{total}$) for $(Ni^{II}_{0.38}Mn^{II}_{0.62})_{1.5}[Cr^{III}(CN)_6]$ based on the three-sublattice molecular field theory. (*b*) Schematic diagram illustrating positive ($M_{Ni} + M_{Cr}$: ■) and negative magnetizations ($M_{Mn}$: □) versus the direction of the external magnetic field at $T > T_{comp}$ and $T < T_{comp}$, respectively.

of the $(Ni^{II}_x Mn^{II}_{1-x})_{1.5}[Cr^{III}(CN)_6] \cdot zH_2O$ series can be predicted using an MF model which considered only superexchange interactions between the nearest neighbours ($Ni^{II}$–$Cr^{III}$ and $Mn^{II}$–$Cr^{III}$).

These results show that in Prussian blue analogues both the ferro- and antiferromagnetic interactions exist simultaneously without spin glass behaviour and their magnetic properties can be explained by MF theory.

## 3. A design of fickle magnet which switches pole direction twice with increasing temperature

Here we will show how well the MF theory works for the design of a novel magnet with Prussian blue analogues by designing a magnet that flips the orientation of its magnetic field twice as its temperature is increased. In other words, this magnet possesses two compensation temperatures (see Ohkoshi *et al.* 1999*a*).

The key objective here is to design Prussian blue analogues containing one ferromagnetic and two antiferromagnetic interactions simultaneously by incorporating four different metal ions into the lattice, three of them being randomly distributed, with the correct ratio being obtained by use of a calculation based on MF theory. We choose members of a new class of mixed ferro-ferrimagnets with the generic formula $(Ni^{II}_a Mn^{II}_b Fe^{II}_c)_{1.5}[Cr^{III}(CN)_6] \cdot z\ H_2O$ $(a + b + c = 1)$ (figure 7).

First, we evaluate theoretically the temperature dependencies of a series of compounds $(Ni^{II}_a Mn^{II}_b Fe^{II}_c)_{1.5}[Cr^{III}(CN)_6] \cdot zH_2O$ using the MF theory, with the spin numbers for the four sublattice sites: $S_{Ni} = 1$; $S_{Mn} = 5/2$; $S_{Fe} = 2$ and $S_{Cr} = 3/2$. For this calculation, only the three types of superexchange couplings between the nearest-neighbour sites, Ni–Cr, Mn–Cr and Fe–Cr, are considered. The molecular fields $H_{Ni}$,

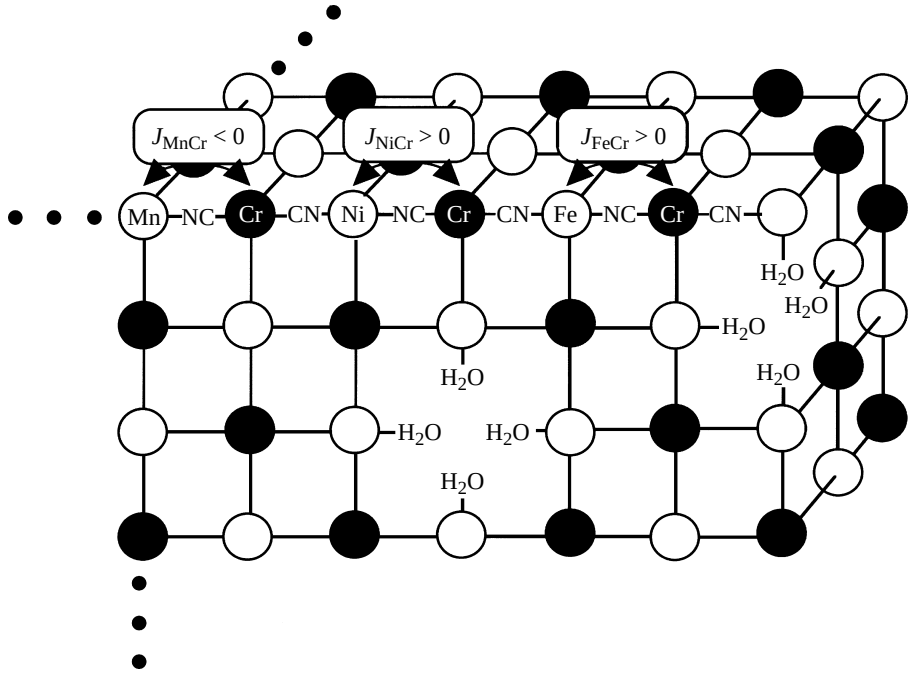


Figure 7. Schematic of mixed ferro-ferrimagnets composed of $(Ni^{II}_a Mn^{II}_b Fe^{II}_c)_{1.5}[Cr^{III}(CN)_6]\cdot zH_2O$. Zeolitic water molecules in the unit cell are omitted for clarity. The ferromagnetic ($J_{NiCr} > 0$ and $J_{FeCr} > 0$) and antiferromagnetic ($J_{MnCr} < 0$) superexchange interactions can coexist without spin frustration, because the $A^{II}$ (A = Ni, Mn or Fe) (○) and $Cr^{III}$ (●) ions of the Prussian blue structure are linked in an alternating fashion. $(Fe^{II}_x Cr^{II}_{1-x})_{1.5}[Cr^{III}(CN)_6]\cdot zH_2O$.

$H_{Mn}$, $H_{Fe}$ and $H_{Cr}$ acting on the four sublattice sites can be expressed as follows:

$$H_{Mn} = H_0 + n_{MnCr}M_{Cr}, \tag{3.1}$$
$$H_{Ni} = H_0 + n_{NiCr}M_{Cr}, \tag{3.2}$$
$$H_{Fe} = H_0 + n_{FeCr}M_{Cr}, \tag{3.3}$$
$$H_{Cr} = H_0 + n_{CrMn}M_{Mn} + n_{CrNi}M_{Ni} + n_{CrFe}M_{Fe}, \tag{3.4}$$

where $H_0$, $n_{ij}$, $J_{ij}$, $M_{Ni}$, $M_{Mn}$, $M_{Fe}$ and $M_{Cr}$ are defined similar to those in § 2. The sublattice magnetizations and total magnetization ($M_{total} = -M_{Mn} + M_{Ni} + M_{Fe} + M_{Cr}$) as a function of temperature can be evaluated using a Brillouin function. A $J_{MnCr}$ value of $-2.5\ cm^{-1}$, a $J_{NiCr}$ value of $+5.6\ cm^{-1}$ and a $J_{FeCr}$ value of $+0.9\ cm^{-1}$ are obtained from the experimental $T_c$ values of

$$Mn^{II}_{1.5}[Cr^{III}(CN)_6]\cdot 7.5H_2O \qquad (T_c = 67\ K),$$
$$Ni^{II}_{1.5}[Cr^{III}(CN)_6]\cdot 8H_2O \qquad (T_c = 72\ K),$$
$$Fe^{II}_{1.5}[Cr^{III}(CN)_6]\cdot 7.5H_2O \qquad (T_c = 21\ K),$$

respectively. Using these $J$ values and the compositional factors ($a$, $b$, $c$), the temperature dependencies are evaluated theoretically. Figure 8 shows the calculated temperature dependence curves for each sublattice and the total magnetization for

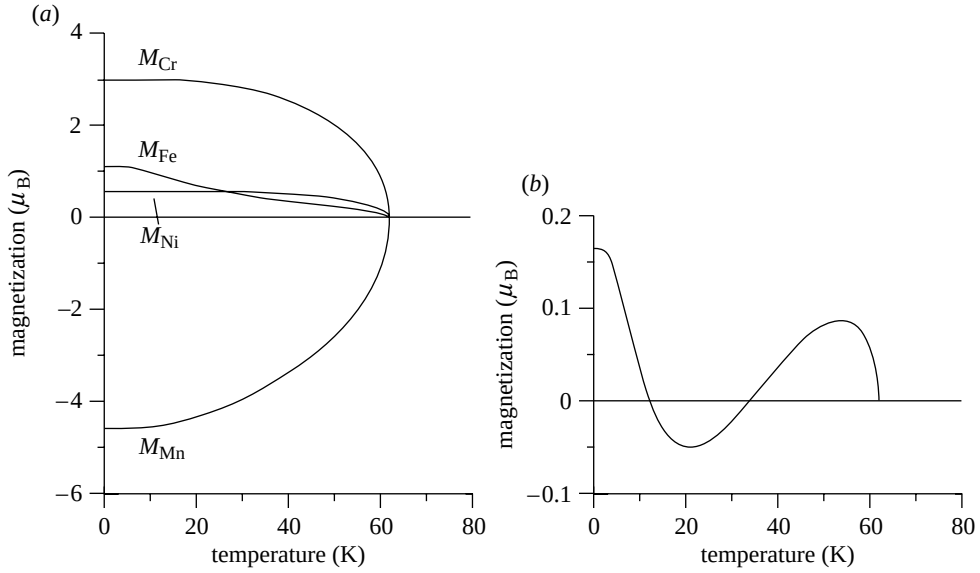


Figure 8. Calculated temperature-dependence curves for each sublattice and total magnetization for $(Ni^{II}_{0.20}Mn^{II}_{0.61}Fe^{II}_{0.19})_{1.5}[Cr^{III}(CN)_6] \cdot zH_2O$, based on molecular field theory, with four sublattice sites (Ni, Mn, Fe, Cr), with $J$ coefficients $J_{NiCr} = +5.6\ cm^{-1}$ , $J_{FeCr} = +0.9\ cm^{-1}$ and $J_{MnCr} = -2.5\ cm^{-1}$: (*a*) sublattice magnetization ($M_{Mn}$, $M_{Ni}$, $M_{Fe}$, $M_{Cr}$); and (*b*) total magnetization ($M_{total}$).

the $(Ni^{II}_{0.20}Mn^{II}_{0.61}Fe^{II}_{0.19})_{1.5}[Cr^{III}(CN)_6] \cdot zH_2O$ system, which exhibits two compensation temperatures. On the basis of this theoretical prediction, we will synthesize members of this series.

The compounds can be prepared by reacting mixtures of $NiCl_2$, $MnCl_2$ and $FeCl_2$ aqueous solutions with $K_3Cr(CN)_6$ aqueous solution to yield light brown precipitates. Similar to the ternary metal Prussian blue analogues, $Ni^{II}$, $Mn^{II}$ and $Fe^{II}$ are randomly incorporated in sites where they are coordinated to the nitrogen ends of the cyano groups, and the $Cr^{III}$ ions are always coordinated to the carbon ends of the cyano groups.

Figure 9 shows the field-cooled magnetization (FCM) versus temperature plots for the $(Ni^{II}_{0.22}Mn^{II}_{0.60}Fe^{II}_{0.18})_{1.5}[Cr^{III}(CN)_6] \cdot 7.6H_2O$ powder in an external magnetic field of 10 G. This compound shows two compensation temperatures ($T_{comp1} = 53$ K and $T_{comp2} = 35$ K). Its remnant magnetization versus temperature plots also show a similar behaviour. The theoretical calculation described above shows clearly that the two compensation temperatures for this compound are due to different temperature dependencies of the negative magnetization of the $Mn^{II}$ sublattice and the positive magnetizations of the $Ni^{II}$, $Fe^{II}$ and $Cr^{III}$ sublattices. In the temperature range between 61 K ($T_c$) and 53 K, the positive magnetizations dominate. Between 53 K and 35 K, however, the negative magnetization outweighs the positive magnetizations. At temperatures below 35 K, the positive magnetizations again dominate due to the growth of the $Fe^{II}$ sublattice contribution. Other magnetic properties also obey the theory of the mixed ferro-ferrimagnetism described in § 2. For example, the $I_s$ value for the composition $a = 0.24$, $b = 0.58$, $c = 0.18$ is $0.77\mu_B$, assuming the $g$ factors for the metal ions to be 2.0. This observed value is close to the theoretical $I_s$

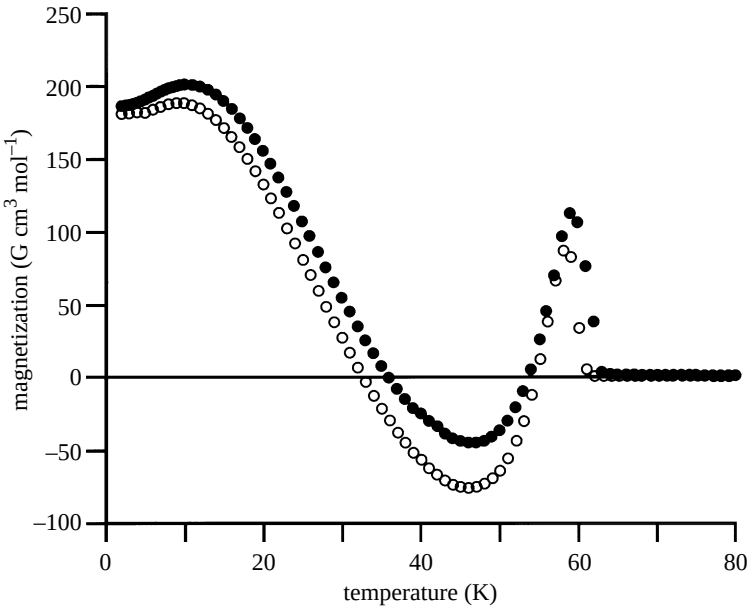


Figure 9. Experimental magnetization versus temperature curves for $(Ni^{II}_{0.22}Mn^{II}_{0.60}Fe^{II}_{0.18})_{1.5}[Cr^{III}(CN)_6] \cdot 7.6H_2O$: (•) field-cooled magnetization obtained with decreasing temperature (80 → 2 K) in an external magnetic field of 10 G; (○) remnant magnetization obtained with increasing temperature (2 → 80 K) after the temperature was first lowered in the applied magnetic field of 10 G.

value of $0.52\mu_B$. In addition, the coercive field ($H_c$) value of 570 G was larger than the $H_c$ values for the respective binary compositions

$$Mn^{II}_{1.5}[Cr^{III}(CN)_6] \cdot 7.5H_2O \qquad (H_c = 6\ \text{G}),$$
$$Ni^{II}_{1.5}[Cr^{III}(CN)_6] \cdot 8H_2O \qquad (H_c = 120\ \text{G}),$$
$$Fe^{II}_{1.5}[Cr^{III}(CN)_6] \cdot 7.5H_2O \qquad (H_c = 200\ \text{G}).$$

This is because the $H_c$ values for the mixed ferro-ferrimagnets are proportional to $I_s^{-1}$.

It is rather surprising that the compound, whose molecular composition is determined based on a simple magnetic theory (MF theory), gives such a complicated magnetic behaviour, possessing two compensation temperatures. This result shows that MF theory is useful for the design of novel magnets in the series of Prussian blue analogue.

## 4. Coloured magnetic thin films

Here we will show the design of various coloured transparent magnetic thin films (Ohkoshi *et al*. 1998). The key to this strategy is to control of the intervalence transfer bands of metal ions in a dye material exhibiting ferromagnetism. We prepared new classes of transparent magnetic thin films composed of $(Fe^{II}_xCr^{II}_{1-x})_{1.5}[Cr^{III}(CN)_6] \cdot zH_2O$. Their colours could be controlled by controlling the compositional factor $x$ $(= Fe^{II}/(Fe^{II} + Cr^{II}))$, e.g. colourless ($x = 0$), violet ($x = 0.20$), red ($x = 0.42$) and

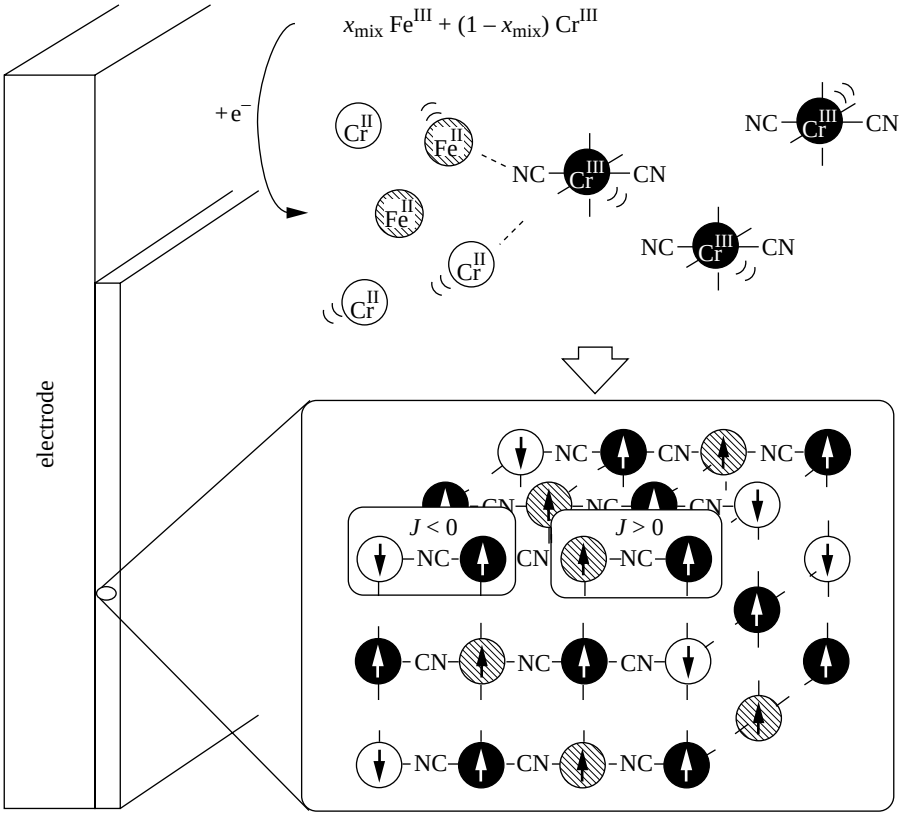


Figure 10. Schematic diagram illustrating electrochemical synthesis of magnetic thin films with both ferromagnetic ($J > 0$) and antiferromagnetic ($J < 0$) interactions. $Cr^{III}$ (black spheres) and either $Fe^{II}$ (hatched spheres) or $Cr^{II}$ (white spheres), which are randomly incorporated in the lattice, are linked in an alternating fashion.

orange ($x = 1$). It should be emphasized that the strategy of this work is essentially different from the electrochromism. Moreover, their magnetic properties are also rich in variety depending on $x$, e.g. disappearance of saturation magnetization, compensation temperatures, and anomalous coercive fields.

The films of ternary metal Prussian blue can be prepared by reducing aqueous solutions containing three compounds $K_3[Cr(CN)_6]$, $CrCl_3$ and $FeCl_3$, where the mixing ratio $x_{mix}$ ($= Fe^{III}/(Fe^{II} + Cr^{II})$) is controlled (figure 10). The $x$ values of the $(Fe^{II}_x Cr^{II}_{1-x})_{1.5}[Cr^{III}(CN)_6]\cdot zH_2O$ series can be controlled either by the $x_{mix}$ values of metal ions in the prepared solutions or by the electrode potential of reducing aqueous solutions.

The magnetic susceptibility and magnetization of obtained thin films depended strongly on the $x$ values. The $I_s$ values for $x = 0$ and $x = 1$ at fields up to 5 T, assuming $g = 2.0$ for metal ions, are determined to be $1.04\mu_B$ and $6.69\mu_B$, respectively. Those for the intermediate compositions vary in a systematic fashion as a function of $x$. Minimum values of the $I_s$ are obtained with the film of $x$ value close to 0.11. This is because the superexchange interaction between $Cr^{III}$ and $Fe^{II}$ are positive (which will be shown in § 6) and that between $Cr^{III}$ and $Cr^{II}$ are negative. Therefore, the

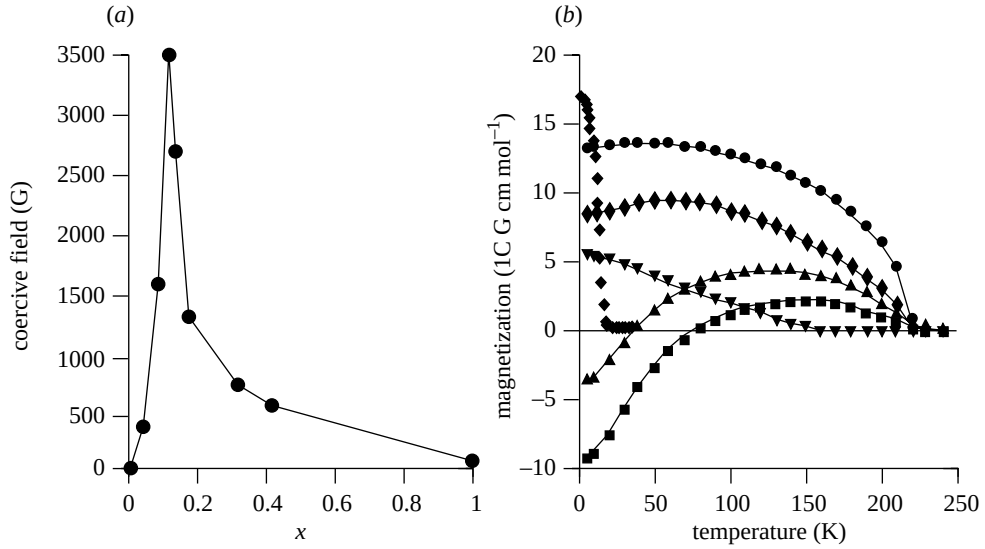


Figure 11. (*a*) Plots of $H_c$ values versus $x$. (*b*) Magnetization versus temperature curves for $(Fe^{II}_x Cr^{II}_{1-x})_{1.5}[Cr^{III}(CN)_6] \cdot zH_2O$ (field of 10 G): (●) $x = 0$; (♦) $x = 0.08$; (▲) $x = 0.11$; (■) $x = 0.13$; (▼) $x = 0.42$; (◆) $x = 1$.

parallel spins ($Cr^{III}$ and $Fe^{II}$) and antiparallel spins ($Cr^{III}$ and $Cr^{II}$) can be partly or even completely cancelled, depending on the $x$ as shown in § 2. Moreover, the $H_c$ value for $x = 0.11$ was much larger than those at the other $x$ values, e.g. 6 G ($x = 0$), 3500 G ($x = 0.11$), and 150 G ($x = 1$) (figure 11*a*). The particle sizes of deposited crystals for the whole $x$ range are almost the same (200–300 nm diameter), so that the $H_c$ values are theoretically expected to be proportional to $I_s^{-1}$. Therefore, the $H_c$ value at minimum $I_s$ value should become the largest. The magnetization versus temperature curves below $T_c$ also exhibit various types of behaviour depending on $x$ (field of 10 G), according to the theory described in § 2 (figure 11*b*). Similar to the other ternary metal Prussian blue systems described previously, these temperature dependencies could be qualitatively reproduced using the molecular field theory, considering only two types of exchange couplings between nearest-neighbour sites, one for $Fe^{II}$–$Cr^{III}$ ($J_{FeCr} = 0.9\ cm^{-1}$) and the other for $Cr^{II}$–$Cr^{III}$ ($J_{CrCr} = -9.0\ cm^{-1}$).

The interesting aspect of the magnetic thin films that were obtained is their optical properties. The colours of $(Fe^{II}_x Cr^{II}_{1-x})_{1.5}[Cr^{III}(CN)_6] \cdot zH_2O$ transparent films are changed depending on $x$. For example, the film for $x = 0$ is colourless, that for $x = 0.20$ is violet, that for $x = 0.42$ is red, and that for $x = 1$ is orange. Their colours are due to the charge transfer (CT) band of $Fe^{II}$ and $Cr^{III}$ in the visible region (see Ludi & Güdel 1973), which is characteristic of mixed-valence compounds. As shown in figure 12, their CT bands shift from short to long wavelength in the visible region with decreasing $x$; e.g. $\lambda_{max} = 434$ nm ($x = 1$); 496 nm ($x = 0.42$); 506 nm ($x = 0.20$); 510 and 610 nm ($x = 0$) and hence their films exhibit various types of colour. In general, the wavelength of CT band depends on magnitudes of the vibronic coupling with asymmetrical distortion of each coordination sphere of metal ions and the intensity is proportional to the square of transfer integrals (see Robin & Day 1967; Hush 1967). Therefore, in a series of $(Fe^{II}_x Cr^{II}_{1-x})_{1.5}[Cr^{III}(CN)_6]$ films, magnitudes of

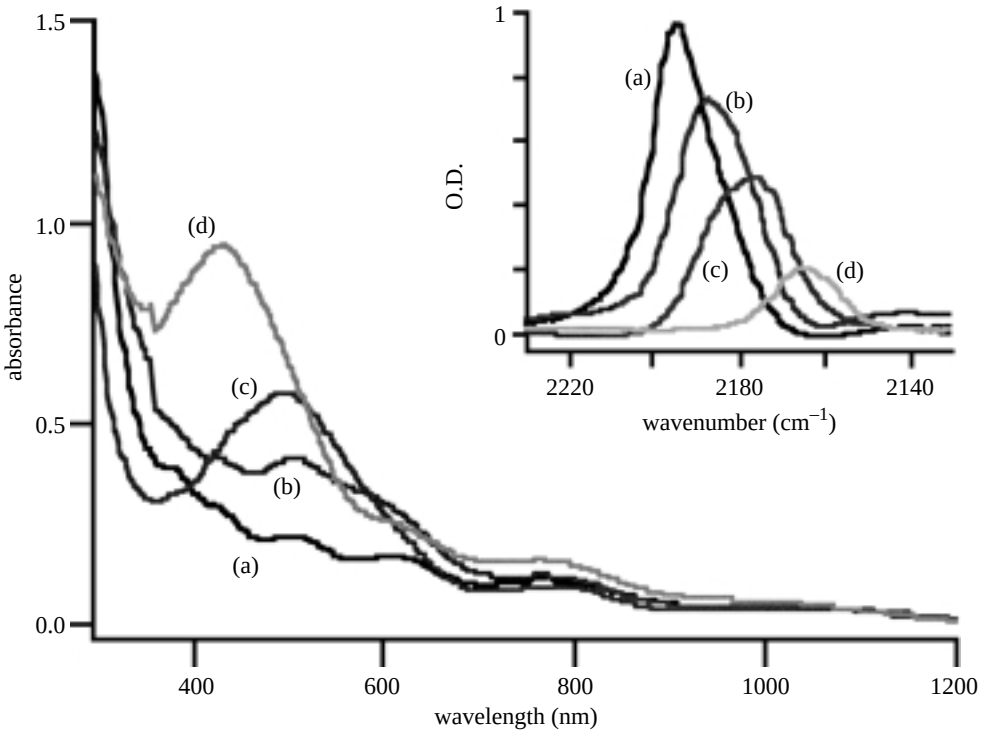


Figure 12. UV–vis and IR spectra of $(Fe^{II}_{x}Cr^{II}_{1-x})_{1.5}[Cr^{III}(CN)_6]\cdot zH_2O$: (*a*) $x = 0$; (*b*) $x = 0.20$; (*c*) $x = 0.42$; (*d*) $x = 1$. IR spectra are shown in the inset.

vibronic coupling parameters and transfer integrals are supposed to be continuously changed from those of $Fe^{II}$–$Cr^{III}$ to those of $Cr^{II}$–$Cr^{III}$ with decreasing $x$. In fact, frequencies of CN stretching and lattice constants also continuously shift, indicating that distances between metal ions of $(Fe^{II}_{x}Cr^{II}_{1-x})_{1.5}[Cr^{III}(CN)_6]$ are averaged values of the distance of $Fe^{II}$–$Cr^{III}$ and $Cr^{II}$–$Cr^{III}$ as a function of $x$.

We can thus design the various types of coloured magnetic thin films composed of Prussian blue analogues incorporating three or more types of metal ions. Here, note that our strategy to tune colour is essentially different from the electrochromism. Of course, when electrochemical reduction or oxidation of our thin films is performed on the electrode, each of thin films exhibits different types of colour and magnetic properties furthermore, e.g. red ($x = 0.42$) to dark blue at $-1.0$ V versus saturated calomel electrode (SCE). In general, the classical magnets show metallic lustre or are black. Here, note that even a yttrium iron garnet used as a photoisolater is seen to be black. Therefore, transparent and coloured magnets will enable one to develop new types of functional thin films.

## 5. Photomagnet

Here we demonstrate the photoinduced reversible change between paramagnet and ferrimagnet in a thin film of $K_{0.4}Co^{II}_{0.3}Co^{III}[Fe^{II}(CN)_6]\cdot 5H_2O$ (see Sato *et al*. 1996, 1997*a*, *b*; Einaga *et al*. 1997). The sodium complex of the cobalt iron cyanide thin film (of thickness *ca*. 0.05–0.1 μm), $Na_{1.4}Co^{II}_{1.3}[Fe^{II}(CN)_6]\cdot 5H_2O$, is first synthesized elec-

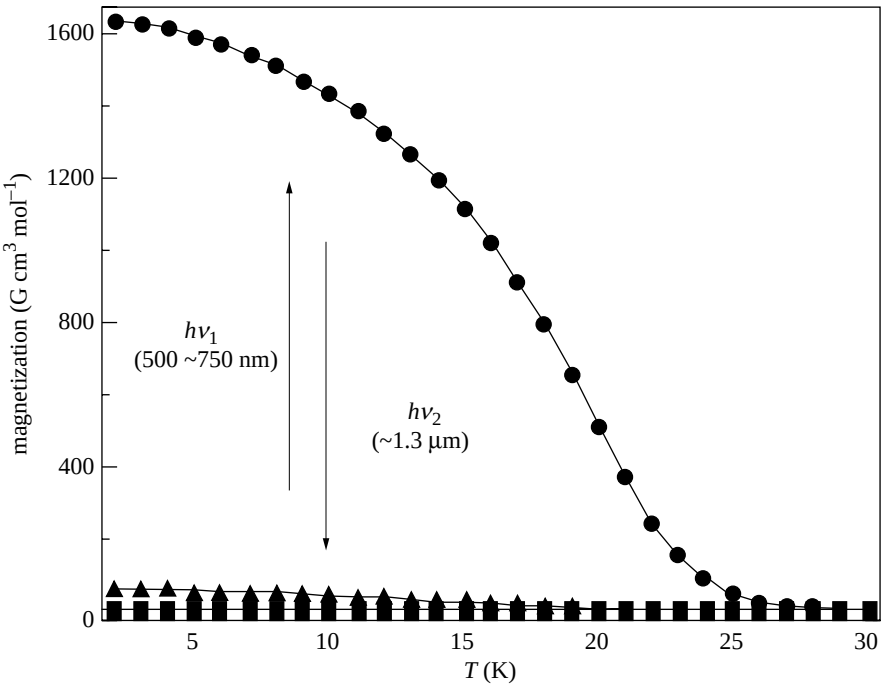


Figure 13. Field-cooled magnetization versus temperature curves for $K_{0.4}Co^{II}_{0.3}Co^{III}[Fe^{II}(CN)_6]\cdot 5H_2O$ at $H = 5$ G; ■, before illumination; ●, after visible light illumination; ▲, after near-IR light illumination.

trochemically on a Pt electrode by reducing $K_3Fe^{III}(CN)_6$ in the presence of $Co^{II}NO_3$ in an aqueous solution of $NaNO_3$ electrolyte. Then this film is electrochemically oxidized in KCl solution, resulting in a formation of $K_{0.4}Co^{II}_{0.3}Co^{III}[Fe^{II}(CN)_6]\cdot 5H_2O$. The absorption spectrum shows a strong, broad absorption band around 550 nm, assigned to the CT band from $Fe^{II}$ to $Co^{III}$.

This compound exhibits an electron transfer from $Fe^{II}$ to $Co^{III}$ involving a spin transition around 340 K. The product of the molar magnetic susceptibility and temperature ($\chi_M T$) versus $T$ plot decreases slightly from 1.3 cm$^3$ mol$^{-1}$ K at 300 K to 0.8 cm$^3$ mol$^{-1}$ K at 20 K. Plots of FCM versus $T$ at a magnetic field of 5 G do not exhibit abrupt breaks in the temperature range between 340 K and 2 K (figure 13). Long-range magnetic ordering is prevented by the presence of a large amount of diamagnetic components of $Fe^{II}$ and $Co^{III}$, whereas the paramagnetic components of $Co^{II}$ are responsible for the paramagnetic character of the compound.

When a red light is used to excite the CT band at 5 K, an increase of the magnetization value is observed. The FCM versus $T$ plots after illumination for 10 min at 5 K show an abrupt break around 26 K (figure 13), indicating three-dimensional, long-range magnetic ordering. The increase in the value of $T_c$ is explained by an increase in the number of magnetic neighbours. The plots of magnetization versus external field at 2 K before illumination do not show hysteresis loops, but those after illumination show the clear presence of hysteresis loops with a remnant magnetization of about 3800 cm$^3$ mol$^{-1}$ G and $H_c$ of about 6000 G at 2 K (figure 14). These results demonstrate that the paramagnetic material is converted to a magnetic one

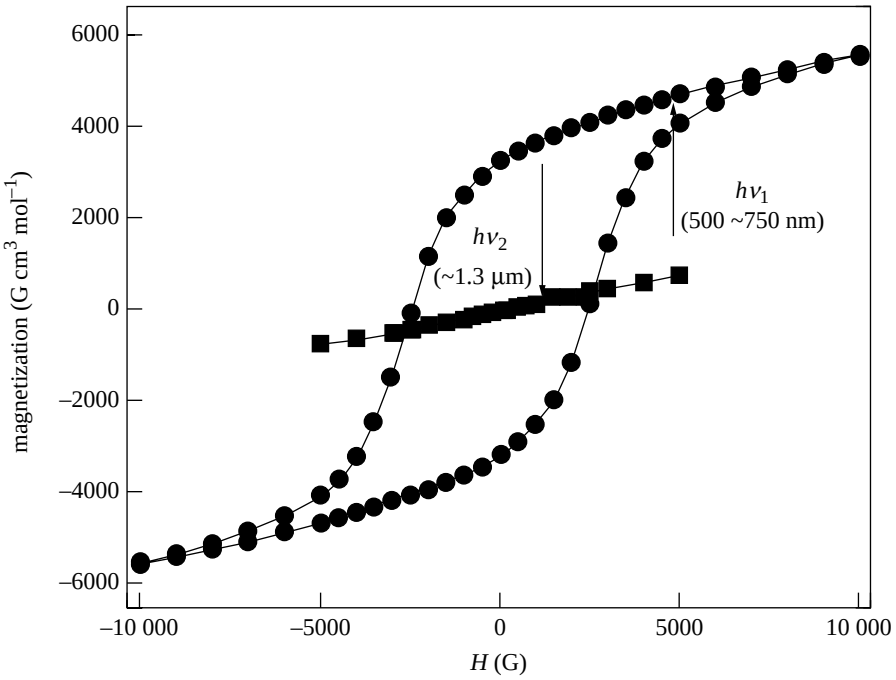


Figure 14. Hysteresis loops for $K_{0.4}Co^{II}_{0.3}Co^{III}[Fe^{II}(CN)_6] \cdot 5H_2O$ at 2 K; ■, before illumination; ●, after visible light illumination; ▲, after near-IR light illumination.

by light illumination. The change persists for periods of several days at 5 K. When the temperature of the sample is raised to 150 K, the magnetic properties quickly relax to almost the initial state.

After illumination, a new absorption peak appears at 400 nm and the peak intensity at 550 nm decreases, while the IR spectrum at 14 K shows that a peak at 2162 $cm^{-1}$ appears and the peak at 2135 $cm^{-1}$ nearly disappears. The Mössbauer spectrum at 25 K before the illumination shows a singlet absorption peak (figure 15*a*) indicating the presence of only low spin $Fe^{II}$ (figure 15*b*). After illumination, however, a doublet absorption peaks appear, showing that $Fe^{II}$ (low spin) is oxidized to $Fe^{III}$ (low spin) during illumination. Taking into consideration of the above results, the change in the electronic states induced by light illumination is expressed as follows:

$$Co^{III}(t^6_{2g}, S = 0)\text{–NC–}Fe^{II}(t^6_{2g}, S = 0) \rightarrow Co^{II}(t^5_{2g}e^2_g, S = 3/2)\text{–NC–}Fe^{III}(t^5_{2g}, S = 1/2). \quad (5.1)$$

Note that the ratio of nitrogen (CN) coordination and oxygen ($H_2O$) coordination to Co depends on the stoichiometry, by which the ligand field of Co is modified. Furthermore, the uptake of $K^+$ makes possible an interaction between $K^+$ and the Fe–CN–Co framework.

The compound, which is characterized by the $Fe^{III}$–CN–$Co^{II}$ structure, has absorption peaks corresponding to the d–d transition for $Fe^{III}$ and $Co^{II}$ around 400 nm and 1300 nm, respectively. By the excitation of the near-IR band, the magnetization value decreases. In figure 13 are also shown the FCM plots after light illumination at 5 K. The enhanced magnetization resulting from visible light illumination can be

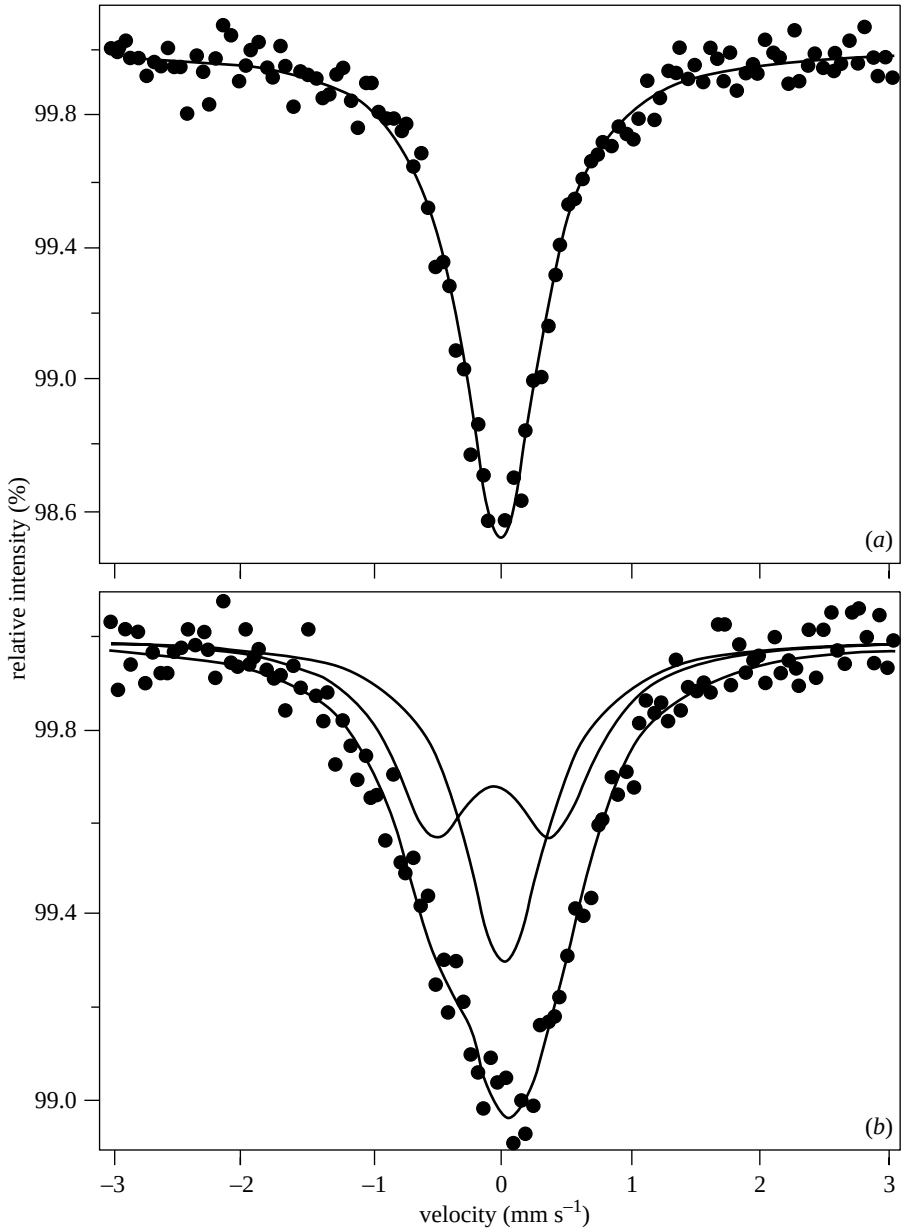


Figure 15. $^{57}$Fe Mössbauer spectra of $K_{0.5}Co_{1.25}[Fe(CN)_6] \cdot 3.6H_2O$ at 25 K (*a*) before and (*b*) after visible light illumination.

almost completely reversed back to the original condition. Similarly, the hysteresis loop almost completely disappears as shown in figure 14. Changes in IR spectra are observed in which the CN stretching peak at 2162 cm$^{-1}$ decreases and a peak around 2135 cm$^{-1}$ increases in intensity, indicates that the reverse process of (3.1) is induced by the near-IR band illumination. The magnetization decreased by the near-IR illumination can then be increased again with visible light. Such a magne-

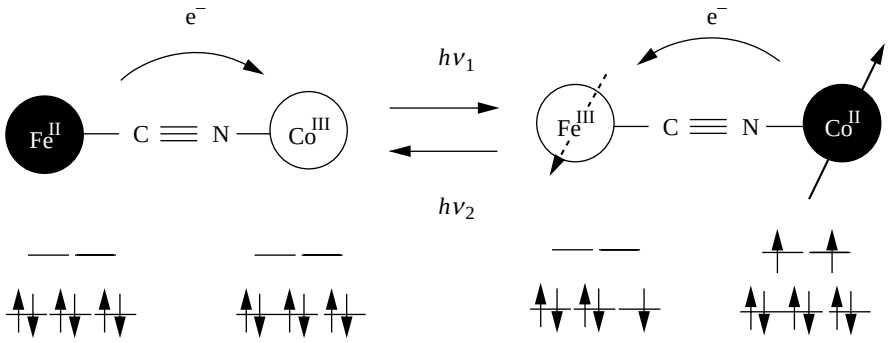


Figure 16. Schematic illustration of photomagnetic behaviour of a Fe–Co Prussian blue analogue based on an electron-transfer mechanism.

tization increase and decrease by visible light, or near IR-light illumination can be reversibly repeated, showing that the magnetic properties of cobalt iron cyanide thin films can be switched between paramagnetic and ferrimagnetic by a photoinduced electron-transfer process (figure 16).

It is interesting to note that such a photomagnet is obtained only with the compounds whose Co and Fe ratio is *ca.* 1.4–1.2. Neither $Co_{1.5}[Fe(CN)_6]\cdot 6H_2O$ (Co:Fe = 1.5:1) nor $KCoFe(CN)_6$ (Co:Fe = 1:1), which is a well-known cobalt–iron cyanide, shows the photoeffects. The Mössbauer and other measurements suggest that the former 1.5:1 compound takes the electronic state of $Co^{II}(t_{2g}^5e_g^2, S = 3/2)$–NC–$Fe^{III}$ $(t_{2g}^5, S = 1/2)$ even without illumination. Conversely, the electronic state of the latter 1:1 compound is $Co^{III}$ $(t_{2g}^6, S = 0)$–NC–$Fe^{II}(t_{2g}^6, S = 0)$, which is the same as that of the photomagnet before illumination, $K_{0.4}Co_{1.3}[Fe(CN)_6]\cdot 5H_2O$, but it does not change on illumination. These results suggest that the energy level of $Co^{III}$–NC–$Fe^{II}$ is situated close to that of $Co^{II}$–NC–$Fe^{III}$ in cobalt iron cyanide, and that they are changed by varying the ratio of Co and Fe. In other words, energy levels can be tuned by introducing defect sites (sites coordinated by water molecules) in the three-dimensional network. For $K_{0.4}Co_{1.3}[Fe(CN)_6]\cdot 5H_2O$, the energy of $Co^{II}$–NC–$Fe^{III}$ is slightly higher than that of $Co^{III}$–NC–$Fe^{II}$, forming a metastable state. This makes it possible to change the electronic state from one to the other reversibly by external stimulation.

## 6. Photo-induced magnetic pole inversion

We here design a novel magnet exhibiting photoinduced magnetic pole inversion by the following strategy. We showed in § 2 that we can control $T_{comp}$ by tuning the mixing ratio of mixed ferro-ferrimagnets composed of Prussian blue analogues. We also showed in § 5 that the $I_s$ value could be changed by photo irradiation for some of the Prussian blue analogues. By introducing such a photosensitive ferro- (or ferri-) magnetic site into a mixed ferro-ferrimagnet showing a negative magnetization, the $T_{comp}$ will be controlled by photostimuli (see Ohkoshi *et al.* 1997*c*; Ohkoshi & Hashimoto 1999*b*). That is, if the photoinduced magnetization changes proceeds at the either ferromagnetic or ferrimagnetic site in a mixed ferro-ferrimagnet, the balance of magnetization between ferromagnetic site and ferrimagnetic site will be upset

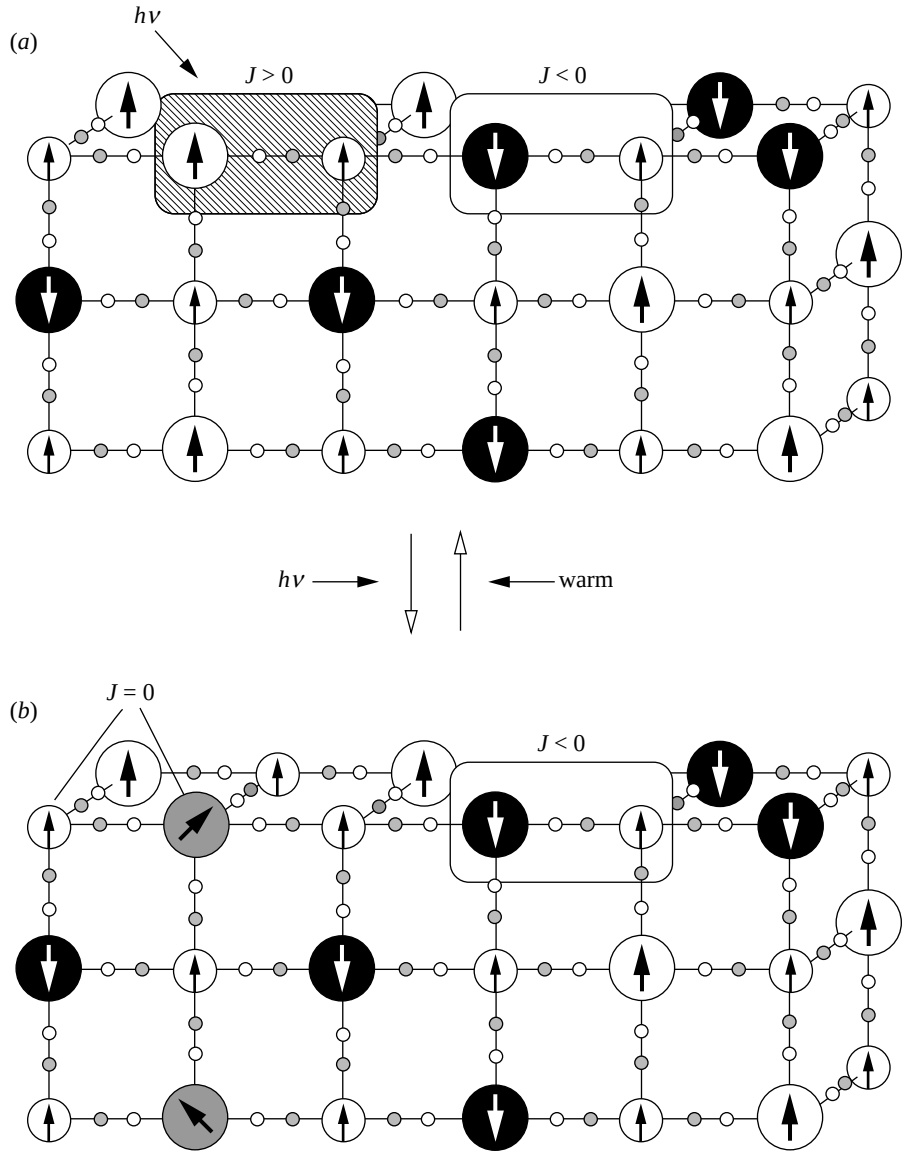


Figure 17. Strategy of photoinduced magnetic pole inversion in mixed ferro-ferrimagnetic Prussian blue analogue, $(Fe^{II}_{x}Mn^{II}_{1-x})_{1.5}Cr^{III}(CN)_6$: (*a*) before irradiation (*b*) after irradiation. The carbon (small grey spheres) ends of the cyano groups are bonded to $Cr^{III}$ (middle small spheres), and the nitrogen (small white spheres) ends are bonded to either $Fe^{II}$ (white spheres) and photoreactive $Fe^{II}$ (grey spheres) or $Mn^{II}$ (black spheres).

by photoirradiation, with the result that the photoinduced magnetic pole inversion is realized at particular temperatures (figure 17).

On the basis of this strategy, we designed an $(Fe_xMn_{1-x})_{1.5}[Cr(CN)_6] \cdot 7.5H_2O$ magnet containing both a ferromagnetic (Fe–Cr) and antiferromagnetic (Mn–Cr) interactions. The $Mn_{1.5}[Cr(CN)_6]{\cdot}7.5H_2O$ for an antiferrimagnetic site has no absorp-

tion in the visible region and hence does not show any change of magnetization by the visible light irradiation. Conversely, the magnetization of $Fe_{1.5}[Cr(CN)_6]\cdot 7.5H_2O$ for a ferromagnetic sites is reduced by the visible light irradiation.

Let us first show the photoinduced magnetization change of this ferromagnetic site. The ferromagnetic interaction between $Fe^{II}$ and $Cr^{III}$ cannot be explained by the orbital symmetry rule described in § 1. However, the FCM plots of $Fe_{1.5}[Cr(CN)_6]\cdot 7.5H_2O$ at $H = 10$ G show an abrupt break at $T_c = 21$ K and the saturated magnetization observed at 5 K is $6.6\mu_B$. Moreover, the $\theta_c$ value estimated from the susceptibility values in the paramagnetic region is 27 K. All these data indicate that this complex is a ferromagnet (Ohkoshi *et al.* 1999*b*). M. Verdaguer (personal communication) suggested that this could be explained by the double-exchange mechanism between these metal ions. However, the estimation of $J_{AF}$ and $J_F$ values between $Cr^{III}$ and $Fe^{II}$ through the CN bond for Prussian blue analogues suggests that $|J_{AF}|$ is almost equal to $|J_F|$. Therefore, contrary to metal oxides, the value of superexchange interaction between $Cr^{III}$ and $Fe^{II}$ could become positive for a Prussian blue analogue even though it contains $J_{AF}$ terms (Ohkoshi & Hashimoto 1999*a*).

As for optical properties, this compound shows the metal ($Fe^{II}$) to metal ($Cr^{III}$) CT band in the visible region ($\lambda_{max} = 454$ nm). By irradiation with a filtered blue light (360–450 nm) at 5 K, the magnetization of $Fe_{1.5}[Cr(CN)_6]\cdot 7.5H_2O$ decreases gradually under the external magnetic field (10 G, 50 G, 500 G, 7 T). About 10% of magnetization is decreased after eight hours irradiation at 10 G. This reduced magnetization persists for a period of several days at 5 K after turning off the light. Note that, in the dark, the magnetization at low temperatures at 10 G does not vary at all by a slight change of the temperature, indicating that this optically induced magnetization change is a photon mode not a photothermal mode. The magnetic property of this illuminated sample returns to the initial one when the temperature of the sample is raised above 30 K, showing that the magnetization can be reduced by a photon mode and recovered by a thermal mode repeatedly. The $^{57}$Fe Mössbauer spectra of the $Fe_{1.5}[Cr(CN)_6]\cdot 7.5H_2O$ before and after irradiation indicate that the spin state of the iron is not changed by irradiation and that neither electron transfer nor spin transition occurs photochemically, but the spins of $Fe^{II}$ and $Cr^{III}$ are no longer aligned after the irradiation. This mechanism is different from that of the Fe–Co photomagnet described in § 5. These results suggest that a ferromagnetic state is converted into a paramagnetic state without changing the valences of the $Cr^{III}$ as a result of the irradiation. This decrease in photoinduced magnetization is explained as follows. The photoexcited state is a mixed valence state of $Cr^{III}$–CN–$Fe^{II}$ and $Cr^{II}$–CN–$Fe^{III}$. This state would relax to a metastable state in which the magnetic interaction is too weak to maintain the spins' ordering. This metastable state is probably stabilized by structural distortion, and returns to the original ferromagnetic state above 40 K.

For the preparation of the Prussian blue analogues incorporating three different metal ions, $(Fe_xMn_{1-x})_{1.5}[Cr(CN)_6]\cdot zH_2O$, an aqueous solution containing both $FeCl_2$ and $MnCl_2$ is added to a concentrated aqueous solution of $K_3[Cr(CN)_6]$, yielding a light-brown-coloured microcrystalline powder. The fraction of $Fe^{II}$ versus ($Fe^{II} + Mn^{II}$) in the above diluted aqueous solution is varied from zero to one, keeping the total metal ion concentration constant.

The magnetic properties of this series agree well with the mixed ferro-ferrimagnetism theory described in § 2. For example, the $I_s$ values at 5 K show a systematic

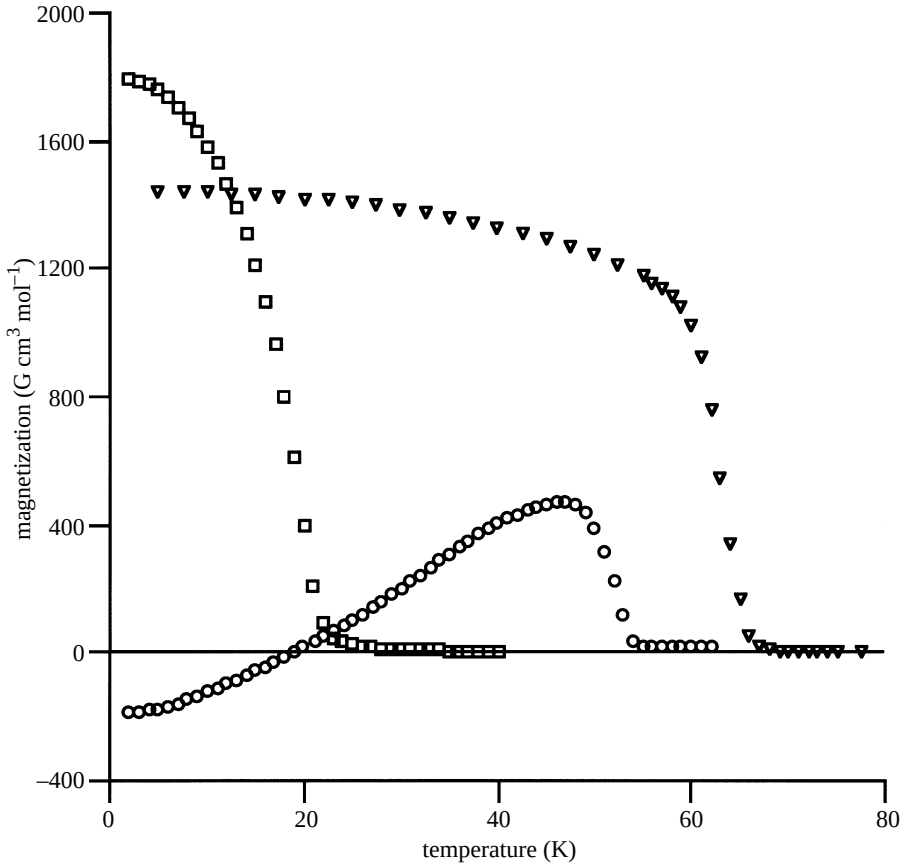


Figure 18. Magnetization versus temperature curves of $(Fe_xMn_{1-x})_{1.5}Cr(CN)_6 \cdot 7.5H_2O$ at 10 G. ($\triangledown$) $x = 0$; ($\circ$) $x = 0.40$; ($\square$) $x = 1$. The temperature dependence of $x = 0.40$ is due to a sum of the positive magnetization of the $Mn^{II}$ sublattice and two negative magnetizations of the $Fe^{II}$ and $Cr^{III}$ sublattices which have different temperature dependencies.

change as a function of $x$, and the values of materials metal ions. In other words, the ferromagnetic coupling between $Fe^{II}$ and around $x \approx 0.4$ is nearly zero. This is because parallel spins ($Cr^{III}$, $S = 3/2$ and $Fe^{II}$, $S = 2$) and antiparallel spins ($Mn^{II}$, $S = 5/2$) cancel depending on the mixing ratio. The $T_c$ values decrease from 67 to 21 K with increasing $x$. In addition, the temperature dependencies of magnetization are rich in variety. Particularly, the material prepared with $x = 0.40$ shows a negative magnetization at low temperature (figure 18).

When the compound for $x = 0.40$ is irradiated at 16 K below $T_{comp}$ with the filtered blue light (360–450 nm), the negative magnetization at 16 K changes gradually to a positive one under the existing external field of 10 G. Simultaneously, the $T_{comp}$ value also shifts to a smaller value and then that disappears, as shown in figure 19. This indicates that the magnetic pole below 19 K is inverted by the optical stimuli. This inverted magnetic pole persists for a period of several days at 16 K after turning off the light. This phenomenon can be explained by the fact that the ratio of the ferromagnetic part (Fe–Cr site) to the antiferromagnetic part (Mn–Cr site) of magnetization of this mixed ferro-ferrimagnet changes due to the decrease of magne-

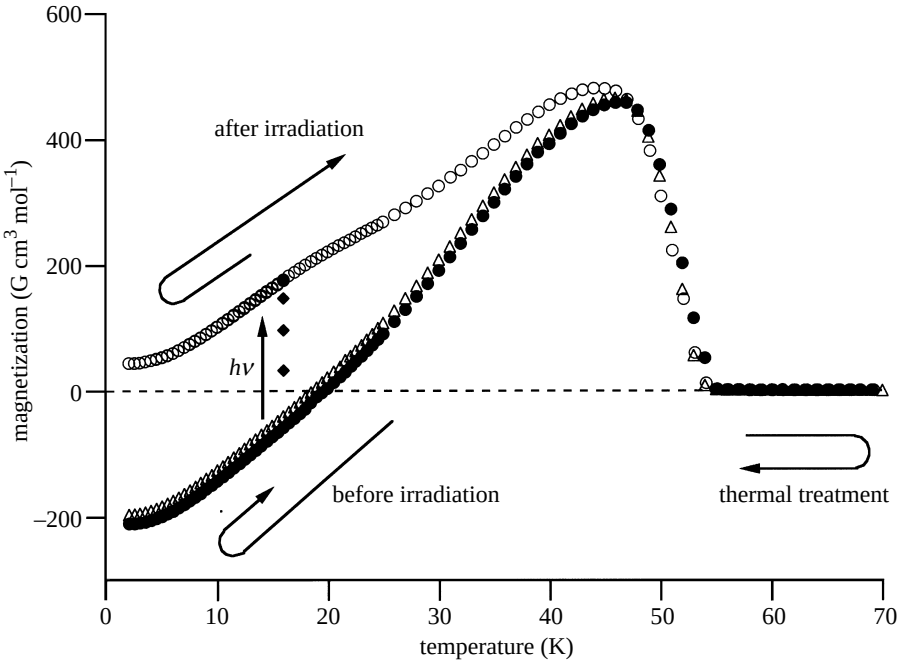


Figure 19. Magnetization versus temperature curves of $Fe_{0.40}Mn_{0.60}Cr(CN)_6 \cdot 7.5H_2O$ in the field of $H = 10$ G before (•) and after (○) light irradiation at 16 K for 72 h. The magnetic pole inversion is observed below the compensation temperature of 19 K by the light irradiation and the pole is reversed back again by the thermal treatment above 80 K (△). Magnetic measurement sequence: 70 K → • → 2 K → • → 16 K (light irradiation for 6, 24, 48, 72 h; ♦) → ○ → 2 K → ○ → 70 K → 80 K (thermal treatment) → 70 K →△→ 2 K.

tization in the ferromagnetic sites. In addition, the magnetization versus temperature curve is recovered by warming to 80 K, indicating that the magnetic pole inversion can be induced repeatedly by alternate optical and thermal stimulation as shown in figure 20.

The phenomenon of photoinduced magnetic pole inversion is used in a photomagnetic recording device made of TbFe, in which the magnetic material is heated above its critical temperature by photoirradiation in the presence of a reverse external magnetic field. During the cooling process below $T_c$, the magnetization arises parallel to the external field, resulting in a pole inversion. However, this phenomenon is induced by a photothermal process, not by a pure photo process. In the present molecule-based magnet, however, the pole inversion is induced by a pure photo process in the absence of an external magnetic field, and thus this process is completely different from that reported previously.

## 7. Conclusion

We have demonstrated various novel magnets, which were designed based on simple theories including a molecular field theory. The reasons why those simple theories can be applicable for the class of Prussian blue analogues are summarized as follows. Firstly, only the superexchange interactions between the nearest-neighbour metal

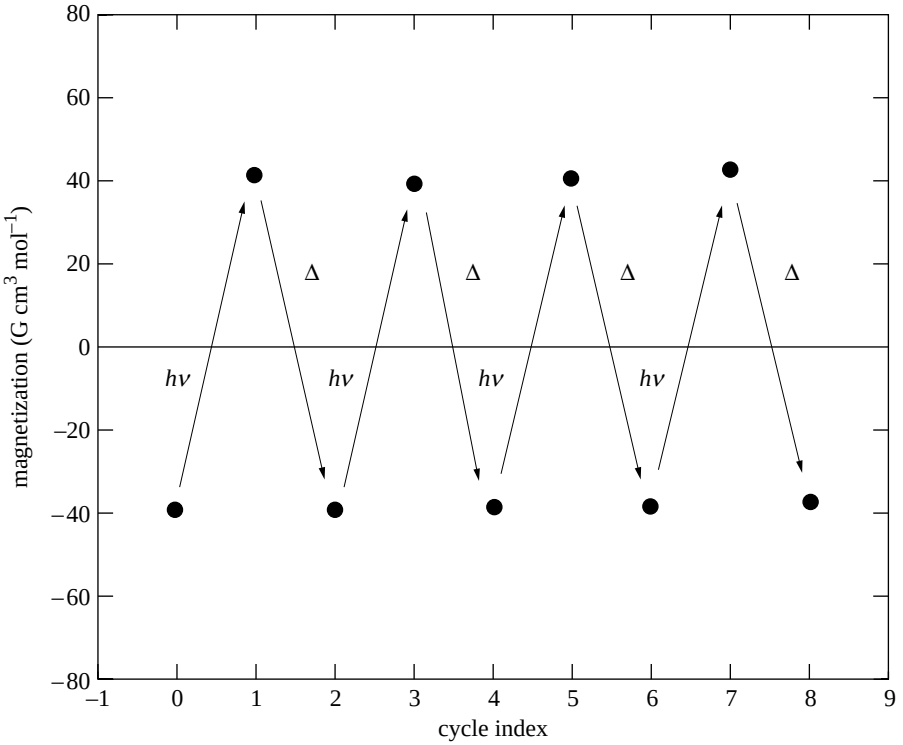


Figure 20. Reversible magnetic pole inversions are demonstrated by alternate stimuli: the magnetization at 15 K after the light illumination ($h\nu$) for 3 h and the magnetization at 15 K after the thermal treatment ($\Delta$) above 80 K.

ions have to be considered. In other words, contributions from the second nearest-neighbour sites can be neglected due to the relatively long distances between metal ions, and hence spin frustration does not occur. Secondly, the face-centred cubic (FCC) crystal structure is always maintained, and the substitution of the metal ion does not change the crystal structure significantly. Thirdly, the character of superexchange interactions can be easily predicted from a simple orbital symmetry rule, because the directions of the symmetry axes of the spin source d-orbitals for all of the metal ion sites and all of the ligand p-orbitals are identical due to their FCC structure. Moreover, a room temperature magnet has been obtained with a Prussian blue analogue (Ferlay *et al*. 1995). We thus believe that Prussian blue analogues will open new avenues in the field of novel magnets.

## References

Anderson, E. E. 1964 Improved molecular field solutions for yttrium and gadolinium iron garnets. In *Proc. Int. Conf. on Magnetism, Nottingham*, p. 660.

Anderson, P. W. 1959 New approach to the theory of superexchange interactions. *Phys. Rev.* **115**, 2.

Einaga, Y., Sato, O., Iyoda, T., Kobayashi, Y., Ambe, F., Hashimoto, K. & Fujishima, A. 1997 Electronic states of cobalt iron cyanides studied by $^{57}$Fe Mössbauer spectroscopy. *Chem. Lett.*, p. 289.

Entley, W. R. & Girolami, G. S. 1994 New three-dimensional ferrimagnetic materials: $K_2Mn[Mn(CN)_6]$,$Mn_3[Mn(CN)_6]_2 \cdot 12H_2O$, and $CsMn[Mn(CN)_6] \cdot \frac{1}{2}H_2O$. *Inorg. Chem.* **33**, 5165.

Ferlay, S., Mallah, T., Ouahes, R., Veillet, P. & Verdaguer, M. 1995 A room-temperature organometallic magnet based on Prussian blue. *Nature* **378**, 701.

Gatteschi, D., Kahn, O., Miller, J. S. & Palacio, F. 1991 *Magnetic molecular materials*. NATO ASI Series E, vol. 198. Dordrecht: Kluwer.

Ginsberg, A. P. 1971 Magnetic exchange in transition metal complexes: aspects of exchange coupling in magnetic cluster complexes. *Inorg. Chim. Acta Rev.* **5**, 45.

Goodenough, J. B. 1958 An interpretation of the magnetic properties of the perovskite-type mixed crystals. *J. Phys. Chem. Solids* **6**, 287.

Goodenough, J. B. 1959 Theory of the role of covalence in the perovskite-type maganites $[La,M(II)]MnO_3$. *Phys. Rev.* **100**, 564.

Gorter, E. W. 1954 Saturation magnetization and crystal chemistry of ferrimagnetic oxides. *Philips Res. Rep.* **9**, 295, 321, 403.

Griebler, W. D. & Babel, D. Z. 1982 Rontgenographische und magnetische Untersuchungen an perowskitverwandten Cyanoverbindungen $CsM^{II}M^{III}(CN)_6$. *Naturforsch.* Teil B **87**, 832.

Hush, N. S. 1967 Intervalence-transfer absorption. Part 2. Theoretical considerations and spectroscopic data. *Prog. Inorg. Chem.* **8**, 391.

Kahn, O. 1993 *Molecular magnetism*. New York: VCH.

Kanamori, J. 1959 Superexchange interaction and symmetry properties of electron orbitals. *J. Phys. Chem. Solids* **10**, 87.

Ludi, A. & Güdel, H. U. 1973 In *Structure and bonding* (ed. J. D. Dunitz), vol. 14, p. 1. Springer.

Mathonière, C., Nuttal, C. J., Carling, S. G. & Day, P. 1994 Molecular-based mixed valency ferrimagnets $(XR_4)Fe^{II}Fe^{III}(C_2O_4)_3$ (X = N, P; R = *n*-propyl, *n*-butyl, phenyl): anomalous negative magnetisation in the tetra-n-butylammonium derivative. *J. Chem. Soc. Chem. Commun.*, p. 1551.

Miller, J. S. & Epstein, A. J. 1994 Organic and organometallic molecular magnetic materials—designer magnets. *Angew. Chem. Int. Ed. Engl.* **33**, 385.

Néel, L. 1948 Proprietes magnetiques des ferrites; ferrimagnetisme et antiferromagnetisme. *Ann. Phys.* **3**, 137.

Nishino, M., Kubo, S., Yoshioka, Y., Nakamura, A. & Yamaguchi, K. 1997 Theoretical studies on magnetic interactions in Prussian blue analogs and active controls of spin states by external fields. *Mol. Cryst. Liq. Cryst.* **305**, 109.

Ohkoshi, S. & Hashimoto, K. 1999*a* Ferromagnetism of cobalt–chromium polycyanides. *Chem. Phys. Lett.* (In the press.)

Ohkoshi, S. & Hashimoto, K. 1999*b* Design of novel magnet exhibiting photo-induced magnetic pole inversion based on molecular field theory. *J. Am. Chem. Soc.* **121**. (In the press.)

Ohkoshi, S., Sato, O., Iyoda, T., Fujishima, A. & Hashimoto, K. 1997*a* Tuning of superexchange couplings in a molecule-based ferroferrimagnet: $(Ni^{II}_xMn^{II}_{1-x})_{1.5}[Cr^{III}(CN)_6]$. *Inorg. Chem.* **36**, 268.

Ohkoshi, S., Iyoda, T., Fujishima, A. & Hashimoto, K. 1997*b* Magnetic properties of mixed ferro-ferrimagnets composed of Prussian blue analogs. *Phys. Rev.* B **56**, 11 642.

Ohkoshi, S., Yorozu, S., Sato, O., Iyoda, T., Fujishima, A. & Hashimoto, K. 1997*c* Photoinduced magnetic pole inversion in a ferro-ferrimagnet: $(Fe^{II}_{0.40}Mn^{II}_{0.60})_{1.5}Cr^{III}(CN)_6$. *Appl. Phys. Lett.* **70**, 1040.

Ohkoshi, S., Fujishima, A. & Hashimoto, K. 1998 Transparent and colored magnetic thin films: $(Fe^{II}_xCr^{II}_{1-x})_{1.5}[Cr^{III}(CN)_6]$. *J. Am. Chem. Soc.* **120**, 5349.

Ohkoshi, S., Abe, Y., Fujishima, A. & Hashimoto, K. 1999*a* Design and preparation of a novel magnet exhibiting two compensation temperatures bed on molecular field theory. *Phys. Rev. Lett.* **82**, 1285.

Ohkoshi, S., Fujishima, A. & Hashimoto, K. 1999*b* Magnetic properties and optical control of iron-chromium polycyanides. *J. Electroanal. Chem.* **473**, 245.

Robin, M. B. & Day, P. 1967 Mixed valence chemistry—a survey and classification. *Adv. Inorg. Chem. Radiochem.* **10**, 247.

Sato, O., Iyoda, T., Fujishima, A. & Hashimoto, K. 1996 Photoinduced magnetization of a cobalt iron cyanide. *Science* **272**, 704.

Sato, O., Einaga, Y., Iyoda, T., Fujishima, A. & Hashimoto, K. 1997*a* Cation driven electron transfer involving a spin transition at room temperature in a cobalt iron cyanide thin film. *J. Phys. Chem.* **10**, 3903.

Sato, O., Einaga, Y., Iyoda, T., Fujishima, A. & Hashimoto, K. 1997*b* Reversible photoinduced magnetization. *J. Electrochem. Soc.* **144**, 11.